

A model for understanding the effects of flow conditions on oyster reef development and impacts to wave attenuation

Rebecca E. Stanley^{a,*}, Matthew V. Bilskie^a, C. Brock Woodson^a, James E. Byers^b

^a College of Engineering, University of Georgia, Athens, GA, United States

^b Odum School of Ecology, University of Georgia, Athens, GA, United States

ARTICLE INFO

Keywords:

Oyster reefs
Nature-based infrastructure
Natural and nature-based features
Numerical modeling
ADCIRC

ABSTRACT

Nature-based solutions (NBS) can be used as an alternative or in conjunction with conventional coastal defense infrastructure for flood hazard mitigation. NBS can provide resilience and ancillary benefits, such as ecosystem enhancement. Oyster reefs, an example of NBS, act as natural breakwaters and provide ecological habitat for numerous species. The effectiveness of oyster reefs as NBS depends on their growth and survival and is influenced by the surrounding hydrodynamic conditions that affect food flux and sedimentation. A point-based oyster growth model was expanded and linked with a hydrodynamic model to simulate oyster and reef growth in the South Atlantic Bight. The highest live oyster layer heights increase with velocity until a depth-dependent velocity threshold is met, where sediment deposition begins to reduce growth. The potential for wave dissipation (total reef height) is depth-limited with a broader range of favorable locations than consideration for oyster layer height alone. The reef heights predicted across the model domain were shown to reduce significant wave height across a range of tropical storm intensities.

1. Introduction

The ability of coastal environments to resist disturbance and adapt is crucial (Folke, 2006; Walker et al., 2004). Traditionally, resistance and adaptation to disturbances has been achieved through the use of ‘grey’ infrastructure, such as seawalls, dikes, and breakwaters, which have long been the primary means of shoreline protection (Schoonees et al., 2019). However, the ecological consequences of these structures, including habitat loss (Dugan et al., 2018), erosion (Dugan et al., 2012; Nordstrom, 2014), biodiversity loss (Aguilera et al., 2019), and reduced thermal heterogeneity, have led to a growing interest in nature-based solutions as an alternative approach. In contrast to grey infrastructure, nature-based solutions combine ecosystem services with coastal protection, offering flood risk reduction and promoting sediment accumulation (Shepard et al., 2011) while providing ecological benefits, including enhanced vertical biomass and adaptability to climate change (Morris et al., 2018).

As a nature-based solution, living shorelines utilize natural ecosystem processes and habitats to provide shoreline protection (Davis et al., 2015). Oyster reef living shorelines, a type of nature-based solution, function as natural breakwaters, delivering both shoreline

protection and ecological benefits (Meyer et al., 1997; Scyphers et al., 2011). As a keystone species (Kennedy et al., 1996; Zu Ermgassen et al., 2012), the Eastern Oyster, *Crassostrea virginica*, plays a critical role in denitrification (Kellogg et al., 2013), estuarine turbidity reduction (Newell and Koch, 2004), and habitat provision for marine organisms (Byers et al., 2017). Oyster reefs provide interstitial living space (Byers et al., 2017), enhancing landscape diversity and act as foraging grounds for predators (Breitburg, 1999; Grabowski, 2004; Meyer et al., 1997). Furthermore, the eastern oyster is a prolific filter feeder (Fulford et al., 2007), filtering large volumes of water which influences nutrient cycling and removes excess nutrients from estuarine environments (Grabowski et al., 2012; Newell et al., 2005; Smyth et al., 2013)

The physical conditions necessary for oyster reef survival and persistence must be considered when employing oyster reefs as a nature-based solution (Morris et al., 2019). Hydrodynamic conditions adjacent to the reef influence oyster size and density, population persistence, survival, and settlement (Housego and Rosman, 2016). Oyster reefs are typically restored along estuarine intertidal and subtidal zones where the maximum depth is between 3 and 5 m (Housego and Rosman, 2016), where likelihood of success is greatest with higher flow speeds (Lenihan, 1999) and the reef being inundated (covered in water), on average,

* Corresponding author.

E-mail address: rebecca.stanley@uga.edu (R.E. Stanley).

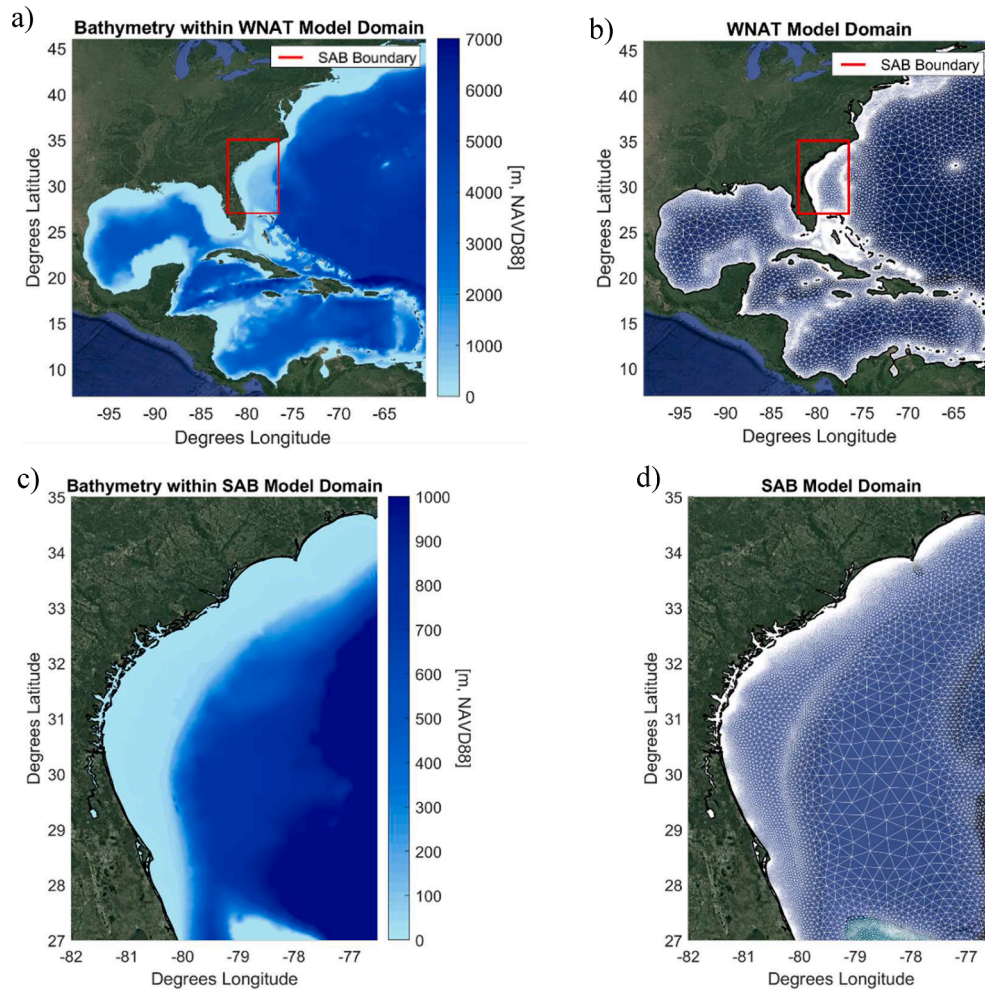


Fig. 1. The WNAT model domain a) bathymetry and b) mesh elements and the South Atlantic Bight (SAB) model domain c) bathymetry and d) mesh elements. The South Atlantic Bight domain boundary within the WNAT domain is outlined in red.

more than 50 % of the time (Housego and Rosman, 2016; Morris et al., 2021).

Flow speed is a critical factor in the survival and mortality of oysters. Flow influences energy expenditure (Fuchs et al., 2015), regulation of food supply (Lenihan, 1999), larval settlement rates (Breitburg et al., 1995), recruitment (Eckman, 1983), and predation (Skilleter and Peterson, 1994). Flow speed substantially influences food availability (Lenihan, 1999; Lenihan et al., 1996), where higher velocities increase food supply, water quality, and possibly nutritional quality, all of which subsequently increase growth rates (Campbell and Hall, 2019; Lenihan, 1999). In contrast, sedimentation can impede growth rates and contribute to mortality, where more energy is required to filter sediment from the water column (Housego and Rosman, 2016) and, in some cases, clogs the gills, resulting in death (Adams et al., 1995). Furthermore, slow growth rates due to insufficient food availability exacerbate the effects of sedimentation (Housego and Rosman, 2016). In such circumstances, the growth of the reef must compete with the sediment accumulation rate, where an inability to do so successfully can lead to burial.

The ability of oysters to withstand environmental pressures such as high-energy flow conditions hinges on the elevation of the reef (Bartol et al., 1999; Wellman et al., 2022). In general, taller reefs display greater resilience and increased oyster density (Schulte et al., 2009) as they experience less sedimentation, less exposure to hypoxia (Lenihan, 1999; Lenihan et al., 1996), and greater tolerance to higher-velocity environments with smaller sediment grain sizes, lower food concentrations, and increased shell degradation rates (Housego and Rosman, 2016).

Conversely, reefs with lower heights exhibit a lower likelihood of survival due to reduced filtration rates, assimilation efficiencies, and greater sedimentation (Housego and Rosman, 2016). The height of the reef itself is dictated by its adjacent hydrodynamic conditions, including flow speed and turbulence, ultimately determining the reef's ability to survive.

The consideration of implementing living shorelines for ecological mitigation and engineering purposes is increasing in coastal areas (Temmerman et al., 2013). Due to gaps in knowledge, the use of oyster reef habitats as nature-based infrastructure has not been widely implemented (Bouma et al., 2014; Feagin et al., 2015). Notably, there is a lack of *in situ* data that measures the effectiveness of restored oyster reef habitats for coastal defense. There is also a lack of literature evaluating how reef development and the subsequent level of shoreline protection offered by oyster reefs are influenced by environmental factors (Morris et al., 2018).

Determining the conditions associated with the reef heights necessary to provide shoreline protection is essential for developing guidelines and a framework for optimal design (Morris et al., 2019). However, a method in predicting reef growth and survival at particular sites with their own associated hydrodynamic conditions does not currently exist. To fill this gap, we present an integration of a hydrodynamic model with an oyster reef growth model developed by Housego & Rosman (2016) to estimate reef growth from spatially and temporally varying bathymetry and flow patterns. In doing so, the expanded model (herein referred to as HR16 + Hydro) is intended to answer three main questions:

- (1) How do oyster reef heights respond to their local hydrodynamic conditions?
- (2) What flow and depth conditions produce the highest reef height and the greatest oyster survival?
- (3) What design frameworks can be created for using oyster reef living shorelines as nature-based infrastructure?

The results predict live oyster layer, dead shell layer, and sediment layer volumes over a thirty-year simulation in response to parameters involving food availability, flow speed, shear stress, erosion, sediment deposition, and shell degradation.

2. Methods

The model presented in this study bridges the gap between oyster reef growth and mortality in response to adjacent hydrodynamic conditions and the spatial heterogeneity of coastal bathymetry and flow patterns. A point-based model developed by Housego & Rosman (2016) (hereafter referred to as HR16) is loosely coupled with a two-dimensional astronomic tide and wind-wave hydrodynamic model. The hydrodynamic model provides bathymetric depths and two-dimensional currents to HR16. Intended as a first-pass adaptation to the HR16 model, this study assesses reef response to hydrodynamic variability.

2.1. Study area

The coupled model simulates the oyster reef response throughout the South Atlantic Bight (Fig. 1), a region of the Atlantic Ocean extending from 27° North at West Palm Beach, Florida, to 35° North at Cape Lookout, North Carolina (Atkinson et al., 1985). This region encompasses most of the Florida east coast, the entirety of the Georgia and South Carolina coast, and the lower portion of the North Carolina coast. It is inhabited by *Crassostrea virginica* (the Eastern Oyster) (Motes et al., 1998). The South Atlantic Bight is characterized by complex shoreline geometry and various types and shapes of estuaries and other shore features (Bacopoulos and Hagen, 2017). The shoreline includes 64 tidal inlets, 40 estuarine rivers, and 3672 km² of intertidal zone, including tidal flats and salt marshes where oyster reefs are commonly found (Bahr and Lanier, 1981; Grabowski et al., 2005).

2.2. Hydrodynamic model

Hydrodynamics were computed using the Advanced CIRCulation (ADCIRC) model. ADCIRC is a barotropic, two-dimensional, unstructured finite element hydrodynamic model that calculates water depths and velocities by solving the depth-averaged form of the shallow water equations (Luettich et al., 1992; Luettich and Westerink, 2004). The unstructured, high-resolution, finite element mesh used in this study contains 1,005,008 elements and 540,114 nodes (Bacopoulos and Hagen, 2017) (Fig. 1). Bounded by the Western North Atlantic Tidal (WNAT) domain westward of the 60-degree West meridian, the mesh includes high-resolution along the coast and within the intertidal zones of the estuaries located in the South Atlantic Bight (Bacopoulos et al., 2011; Bacopoulos and Hagen, 2017). Within the South Atlantic Bight, 86 % of all nodes are located within inshore features, with 56 % being in intertidal areas to accurately simulate tidal flows and energy exchange through the complex creek-marsh network and continental shelf (Blanton et al., 2004).

The seven dominant deep water astronomic tidal constituents were used to force the model across the open-ocean boundary (O_1 , K_1 , Q_1 , M_2 , N_2 , S_2 , and K_2) (Hagen et al., 2006). Tidal forcing was simulated over 45 days with a one-second time step, allowing sufficient duration to capture the frequencies of each astronomical constituent (Bacopoulos and Hagen, 2017). The tides were ramped using a hyperbolic tangent function for the first 10 days of the simulation. The last 35 days of simulated

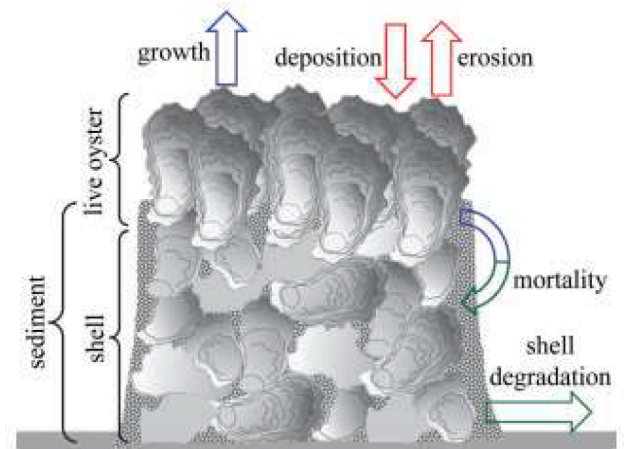


Fig. 2. Oyster reef system structure and processes among and between layers. Adapted from Housego & Rosman (2016).

water levels and currents were used to extract the amplitude and phase for 23 tidal constituents at each mesh node (Giardino et al., 2011). Time-series of the water surface elevation, η , were computed using tidal resynthesis:

$$\eta(t) = \sum_{i=1}^N a_i \cos(\omega_i t + \alpha_i) \quad (1)$$

where t is time, N is the number of tidal constituents (23 for the model, 37 for the observed values) (Bacopoulos et al., 2011), and for each constituent i , a_i is amplitude, ω_i is the angular frequency, and α_i is phase angle. The total water depth, H , was calculated by adding the change in water surface elevation to depth relative to the mean sea level (MSL), h , at each node.

Similarly, the velocity in the x- and y-direction, U_{ix} and U_{iy} , is equal to the magnitude of the summed directional velocities for each tide constituent, where both the x and y velocity for each constituent are contingent upon their corresponding amplitude and phase angle.

$$U_x(t) = \sum_{i=1}^N a_{i,x} \cos(\omega_{i,x} t + \alpha_{i,x}) \quad (2)$$

$$U_y(t) = \sum_{i=1}^N a_{i,y} \cos(\omega_{i,y} t + \alpha_{i,y}) \quad (3)$$

$$U = \sqrt{U_x^2 + U_y^2} \quad (4)$$

2.3. Oyster reef model

The oyster reef model was run for each mesh node in the hydrodynamic model, constrained between -82° to -76° Longitude and 27° – 35° Latitude. Each node's time-varying water depth and flow speed magnitude were used to calculate the responding oyster reef height and sublayer volumes. The oyster reef model assumes a structure as follows, based on Housego & Rosman (2016). The live oyster layer is above the dead shell layer volume, and sediment fills in the gaps between the shells of the live and dead oysters. As adult oysters grow and juveniles are recruited to the reef, the oyster layer volume increases. As oysters perish, the oyster layer volume decreases, and the shell left behind contributes to the dead shell layer volume. The growth in the shell layer is counteracted by shell degradation. Instead of being situated below the reef layer, sediment is assumed to fill in the gaps between the individual shells and individual oysters, and in some cases, fill the reef and begin settling at the top of the oyster layer. Sediment is removed by erosion, decreasing the sediment layer volume (Fig. 2). Because the grain size and sea floor substrate are assumed to be constant, the weight of the reef

Table 1

Parameters and values used in the HR16 model. All values are taken from Housego & Rosman (2016).

ϕ_O	Volume fraction occupied by oysters	0.6	
ϕ_B	Volume fraction occupied by shell	0.6	
ϕ_S	Volume fraction occupied by sediment	0.4	
Q	Individual oyster filtration rate	1 E^{-6}	m^3/s
M	Mean biomass (dry weight) of individual oyster	0.0003	Kg
V	Mean volume of individual oyster	5.6 E^{-5}	m^3
k	Von Karman constant	0.4	
c_f	Ambient food concentration	0.0001	kg/m^3
l	Ratio of respiration to assimilation	0.67	
z_{ref}	Height at reference food concentration	1	M
z_{bed}	Height just above bed	0.01	M
μ	Mortality rate in the absence of sediment	0.4	year^{-1}
ε	Mortality rate of oysters covered in sediment	0.94	year^{-1}
γ	Oyster shell degradation rate	0.2	year^{-1}
d	Sediment grain size	0.0001	M
ρ_w	Density of water	1027	kg/m^3
ρ_s	Density of sediment grains	2650	kg/m^3
ν	Kinematic viscosity of water	1 E^{-6}	$\text{Pa} \cdot \text{s}$
g	Gravity	9.81	m/s^2
a	Some reference height	0.03	M
E_0	Bed erodability constant	29.7509	m/year
θ_c	Critical shields parameter	0.05	m^{-1}
m	Decay rate of shear stress	0.02	
C_D	Drag coefficient at top of reef	0.01	

is assumed to pose no bearing on the risk of land subsidence.

The model utilizes the same governing equations as those in the HR16 model, consisting of three coupled differential equations representing oyster layer volume O_t (Eq. (5)), dead shell layer volume B_t (Eq. (6)), and sediment layer volume S_t (Eq. (7)). The original equations used in the HR16 model have been rearranged to calculate layer volumes at specified timesteps rather than their rate of change, where volume is in units of cubic meters per square meter of area. Parameters and values are provided in Table 1.

$$O_t = \left[\underbrace{\frac{b_1 f(O_{t-1})}{b_2(O_{t-1}) + 1}}_{\text{growth}} - \underbrace{[\mu f + \varepsilon(1-f)]}_{\text{mortality}}(O_{t-1}) \right] \Delta t + (O_{t-1}) \quad (5)$$

$$B_t = \left[\underbrace{[\mu f + \varepsilon(1-f)]}_{\text{mortality}}(O_{t-1}) - \underbrace{\gamma(B_{t-1})}_{\text{degradation}} \right] \Delta t + (B_{t-1}) \quad (6)$$

$$S_t = \left[\underbrace{(C \cdot W_s)}_{\text{deposition}} - \underbrace{E}_{\text{erosion}} \right] \Delta t + (S_{t-1}) \quad (7)$$

In the growth term of the oyster layer volume equation (Eq. (5)), b_1 and b_2 represent non-density dependent and density-dependent growth, respectively. The mortality term is present in both the oyster layer volume equation and the shell layer volume equation (Eq. (6)), where μ is the annual mortality rate of oysters that are not covered by sediment, whereas ε denotes the annual mortality rate due to sediment smothering. The fraction of the live oyster layer not covered by sediment is given by f . In the sediment layer volume equation (Eq. (7)), γ is the annual shell degradation rate, C is the sediment concentration above the reef, W_s is the settling velocity, and E is erosion. All parameters and associated values independent of depth and velocity are consistent with those used in the HR16 model (Table 1).

Growth in the context of the model refers to the growth of the layer volume. The growth represents both adult oysters and juvenile recruitment in a single term. The non-density-dependent growth parameter, b_1 , is the fractional rate of increase without competition and is governed by biological parameters. The b_2 term encompasses growth influenced by the reduction of food concentration due to the oyster population

filtering the surrounding water, where filtering removes food from the water above the reef. Here, it is assumed that the reduction of food supply is counteracted by vertical mixing. As a result, the food concentration profile is logarithmic and increases with height from the bed and is a function of velocity.

Because of the impact of smothering of sediment on fitness (Adams et al., 1995), it is assumed that oysters that are covered by sediment do not contribute to growth. As a result, the fraction of the oyster population not covered by sediment, f , is multiplied by the oyster layer volume so that the oyster growth rate only applies to the oysters that can contribute to reef growth.

The mortality term is the sum of the normal mortality rate per year, μ , and the additional mortality that occurs due to smothering by sediment ε . The mortality rate of oysters in the absence of sediment per year is multiplied by the oyster layer volume times the fraction of the oyster population that is not covered by sediment f . Similarly, the mortality rate of oysters covered in sediment is multiplied by $(1 - f)$, the fraction of oysters that are covered by sediment. The mortality of oysters in the oyster layer, O_t , contributes the shell layer volume. The accumulation of shell is counteracted by the shell degradation term, which is the rate of shell degradation per year, γ , times the shell volume of the previous timestep.

The amount of sediment within the reef is a crucial factor in oyster mortality. The sediment layer volume is equal to the volume of sediment deposited onto the reef, which is a function of the sediment concentration above the reef C and settling velocity W_s , minus the volume removed due to erosion E . Sediment filtered by oysters is not removed from the deposition term, as the sediment is returned to the reef as pseudofeces. The sediment concentration profile is assumed to follow a Rouse sediment concentration profile next to the reef (Housego and Rosman 2016; Eq. (8)), where downward settling and upward turbulent mixing counteract each other (van Rijn, 1993).

$$C = \begin{cases} C_{s,a} \left(\frac{H - (h_O + h_B)}{h_O + h_B} \cdot \frac{a}{H - a} \right)^{W_s/k_{u_* \text{flat}}} & (h_S < h_B) \text{ or } (h_B < h_S < h_B + h_O) \\ C_{s,a} \left(\frac{H - h_S}{h_S} \cdot \frac{a}{H - a} \right)^{W_s/k_{u_* \text{flat}}} & h_S > h_B + h_O \end{cases} \quad (8)$$

If the top of the shell layer is above the top of the sediment layer, the sediment concentration at the top of the reef is equal to the depth integrated sediment concentration $C_{s,a}$ multiplied by the product of the unoccupied water to reef height ratio and some reference height a near the bed to the total water depth minus the reference height ratio, all to the power of settling velocity W_s (Eq. (9)). If the sediment layer is above the top of the shell layer, the ratio of unoccupied water to the reef height is instead the ratio of unoccupied water to the sediment layer height.

$$W_s = \frac{\rho_s - \rho_w}{\rho_w} \frac{g d^2}{18 \nu} \quad (9)$$

$C_{s,a}$, the depth integrated sediment concentration (Eq. (10)), is the product of an intermediate value of total suspended sediment concentration $C_{s,avg}$ (Eq. (11)) recorded by Fugate & Friedrichs (2002) and the integral of Eq. (8), where z is equal the largest of either total reef height $h_B + h_O$, or the sediment layer height h_S .

$$C_{s,a} = C_{s,avg} \left[\int_a^H \left(\frac{H - z}{z} \cdot \frac{a}{H - a} \right)^{W_s/k_{u_* \text{flat}}} dz \right]^{-1} \quad (10)$$

$$C_{s,avg} = 4E^{-6}(H - a) \quad (11)$$

Erosion, E , is dependent upon the relative heights of each layer and only occurs when there is sufficient shear stress to induce sediment motion (Eq. (12)). The Shields parameter θ , a ratio of the effects of shear

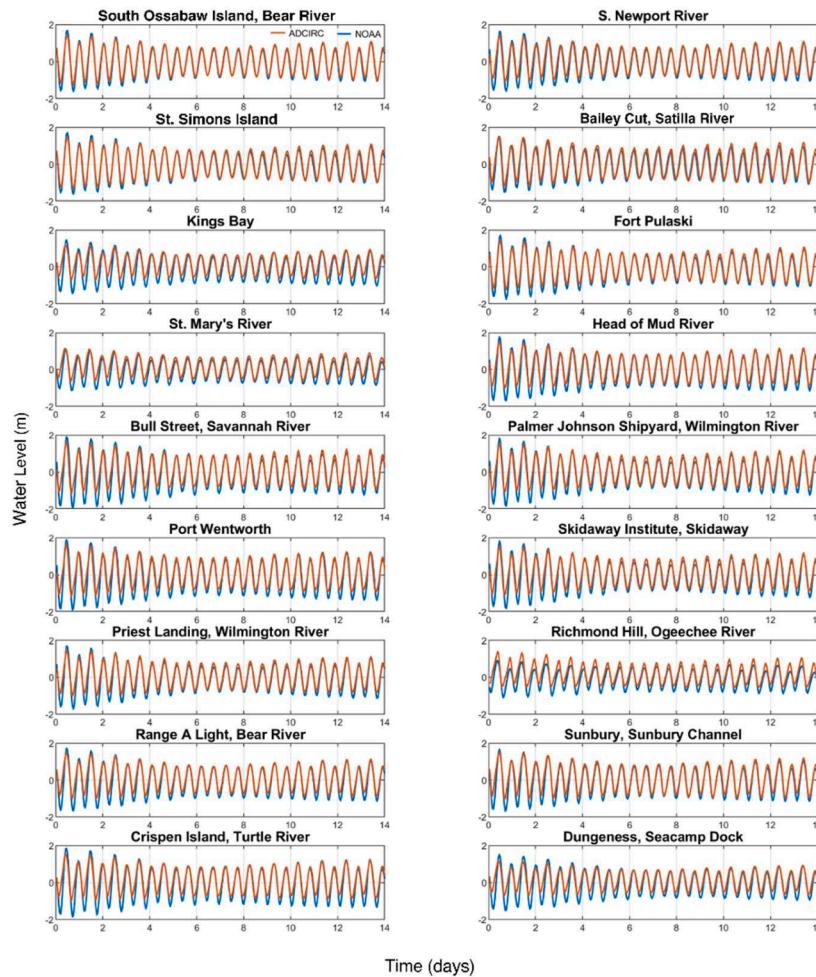


Fig. 4. 14-day tide resynthesis of NOAA observed and ADCIRC simulated tides at a) South Ossabaw Island, Bear River, Georgia; b) S. Newport River, Georgia; c) St. Simons Island, Georgia; d) Bailey Cut, Satilla River, Georgia; e) Kings Bay, Georgia; f) Fort Pulaski, Georgia; g) St. Mary's River, Georgia; h) Head of Mud River, Georgia; i) Bull Street, Savannah River, Georgia; j) Palmer Johnson Shipyard, Wilmington River, Georgia; k) Port Wentworth, Georgia; l) Skidaway Institute, Skidaway, Georgia; m) Priest Landing, Wilmington River, Georgia; n) Richmond Hill, Ogeechee River, Georgia; o) Range A Light, Bear River, Georgia; p) Sunbury, Sunbury Channel, Georgia; q) Crispin Island, Turtle River, Georgia; and Dungeness, Seacamp Dock, Georgia.

stress and the effects of gravitational forces (Shields, 1936) (Eq. (13)), must be greater than the critical Shields parameter θ_c to induce sediment motion. If this condition is not satisfied, or when the shear stress acting on the sediment is not sufficient, erosion is equal to zero. When this condition is met and erosion occurs, it is a function of the shear stress acting on the bed τ_{bed} , the sediment density ρ_s , the water density ρ_w , the gravitational constant g , and is the sediment grain size d .

$$E = \begin{cases} E = E_0 \frac{\theta - \theta_c}{\theta_c} & (\theta < \theta_c) \\ 0 & (\theta > \theta_c) \end{cases} \quad (12)$$

$$\theta = \frac{\tau_{bed}}{(\rho_s - \rho_w)gd} \quad (13)$$

The shear stress acting on the sediment depends on how much, if any, sediment is protected by the reef (Eq. (14)). If the top of the sediment layer is between the live oyster and shell layer, the sediment will be shielded from shear stress acting against the reef. Consequently, the amount of sediment to be eroded decreases, as the shear stress experienced by the sediment decays exponentially with increasing distance from the top of the reef (Whitman and Reidenbach, 2012). However, if the sediment layer is above the top of the reef, the shear stress acting on the sediment is simply a function of friction velocity.

$$\frac{\tau_{bed}}{\rho_w} = u_*^2 = \begin{cases} C_{D,reef} U^2 & h_s > h_B + h_o \\ C_{D,reef} U^2 e^{-\frac{1}{m}(h_o + h_B - h_s)} & h_B < h_s < h_B + h_o \end{cases} \quad (14)$$

2.3.1. Influence of water depth and velocity

Because the growth and mortality terms of the oyster layer equation (Eq. (4)) influence the fraction of oysters not covered by sediment, the relative height of the sediment layer plays a crucial role in determining the reef height and the oysters' ability to survive. Deposition and erosion, the two components of the sediment layer equation, are influenced by water depth and velocity.

The HR16 model assumes constant depth and velocity. However, the HR16 + Hydro model considers the spatial and temporal variations in depth and depth-integrated velocity. HR16 + Hydro performs calculations at each specified node, with depth and velocity being a function of time and the tidal harmonic data obtained from the ADCIRC simulation. Including tidal influence is particularly significant in the intertidal zone, where oyster reefs experience both submergence and emergence. Growth is assumed to be zero for time steps when the oyster reef extends above the water column.

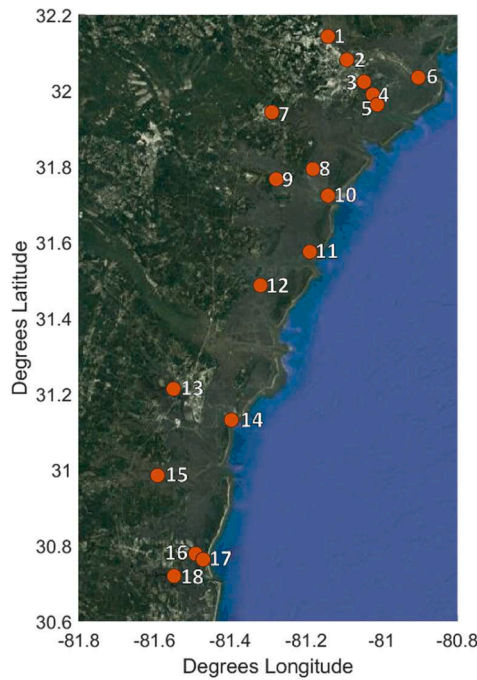


Fig. 3. NOAA stations used in tidal resynthesis. The eighteen stations measure tidal harmonic constituent data. The station name, ID, and coordinates are presented in Table 2.

2.3.2. Model parameters

In the oyster reef model, the governing equations were calculated using MATLAB scripts. The oyster layer volume O_t , shell layer volume B_t , and sediment layer volume S_t were calculated for each mesh node at a 3 h timestep. This timestep was optimal for maintaining accuracy while considering the computational expense of performing the calculations across the model domain. The model has a total run-time of thirty years. To minimize memory usage, the values O_t , B_t , and S_t were saved every 6 months.

The initial conditions for O_t , B_t , and S_t were 0.01 m, 0.13 m, and 0.01 m, respectively, based on Housego and Rosman (2016) to yield the highest steady-state reef height. The initial height corresponds to the mean sea level value. The initial velocity was the magnitude of the x- and y-direction velocity per node at timestep 1. Total water depth H , flow velocity U , change in water level η , oyster layer volume O , shell layer volume B , sediment layer volume S , the fraction of oysters not covered by sediment f , shear stress τ_{bed} , erosion E , and sediment deposition were stored at every 6 months of the simulation.

2.3.3. Assumptions

The HRL16 + Hydro model incorporated several general assumptions from the HRL16 model. Some of these assumptions include a constant water temperature of 30 °C, regardless of the time of day, season, or climate change-related temperature fluctuations. Live oysters were assumed to have a constant size, with a shell length of 80 mm, a volume of 55.7056 mL, and a biomass of 0.3 g (dry weight) per oyster, irrespective of their stage in the life cycle. Mortality was attributed to predation and disease, but these factors are not distinguished in the mortality term of the live oyster layer equation and the dead shell layer equation. Instead, they are combined into one natural mortality rate. While the mortality rate of oysters buried by sediment is constant per volume of oyster, the total mortality due to sediment smothering is volume dependent. In other words, the rate itself was assumed not to change. Finally, the rate of dead shell degradation was assumed to be constant. Like the mortality rate mentioned in the second assumption, dead shell degradation is dependent on dead shell volume, but the rate at which shell degrades is constant (Jordan-Coolley et al., 2011).

Table 2

NOAA stations used in tidal resynthesis as labeled in Fig. 3. The station name associated with each station depicted in Fig. 3 and the corresponding NOAA Station ID and geographic coordinates are presented.

Map ID	Station	NOAA station ID	Longitude	Latitude
1	Port Wentworth	8,670,424	81.1417°	32.1433°
2	Bull Street, Savannah River	8,670,681	81.0917°	32.0817°
3	Palmer Johnson Shipyard, Wilmington River	8,670,893	81.0467°	32.0233°
4	Skidaway Institute, Skidaway	8,671,086	81.0233°	31.9900°
5	Priest Landing, Wilmington River	8,671,315	81.0117°	31.9633°
6	Fort Pulaski	8,670,870	80.9033°	32.0350°
7	Richmond Hill, Ogeechee River	8,671,489	81.2900°	31.9433°
8	Range A Light, Bear River	8,672,667	81.1817°	31.7933°
9	Sunbury, Sunbury Channel	8,672,875	81.2783°	31.7667°
10	South Ossabaw Island, Bear River	8,673,171	81.1417°	31.7233°
11	S. Newport River	8,674,301	81.1900°	31.5750°
12	Head of Mud River	8,674,975	81.3200°	31.4867°
13	Crispen Island, Turtle River	8,676,808	81.5500°	31.2133°
14	St. Simons Island	8,677,344	81.3967°	31.1317°
15	Bailey Cut, Satilla River	8,678,322	81.5917°	30.9850°
16	Kings Bay	8,679,511	81.4917°	30.7783°
17	Dungeness, Seacamp Dock	8,679,758	81.4717°	30.7633°
18	St. Mary's River	8,679,964	81.5483°	30.7200°

The model did not account for human influence on the reef or hydrologic system, such as sea level rise, changes in sediment regime, harvesting, or pollution. It was assumed that there is no competition for space or food with other species, and the reef is inhabited by oysters only - no space is occupied by other species. Lastly, the sediment grain size was assumed to be constant, so sediment deposition depends only on changes in depth and velocity.

3. Results

3.1. Hydrodynamic simulation

The ADCIRC simulation results were validated by constructing a 14-day tide resynthesis using the computed tidal harmonic constituent data and comparing the resulting water surface elevations with observed data collected at eighteen NOAA gages along the Georgia coast (Fig. 4). The NOAA stations measuring harmonic constituent data are displayed in

Table 3

Root mean squared error (cm), MSE/VAR, correlation coefficient (R2), relative bias, and scatter index between the NOAA-observed water levels and ADCIRC-modeled water levels.

Station	RMSE (cm)	MSE/VAR	R ²	Relative bias	SI
South Ossabaw Island	0.708	0.032	0.985	-0.283	-2.177
S. Newport River	1.213	0.094	0.935	-0.825	-3.712
St. Simons Island	0.748	0.038	0.971	-0.316	-2.307
Satilla River	1.256	0.110	0.921	-0.958	-4.161
Kings Bay	1.926	0.292	0.840	-1.778	-5.037
Fort Pulaski	0.902	0.051	0.974	-0.364	-2.204
St. Mary's River	1.450	0.252	0.894	-1.293	-4.865
Head of Mud	1.480	0.121	0.925	-1.216	-4.480
Bull Street	1.812	0.150	0.886	-1.575	-4.743
Palmer Johnson Shipyard	1.538	0.134	0.902	-1.313	-4.658
Port Wentworth	1.860	0.150	0.888	-1.923	-5.641
Skidaway Institute	1.575	0.141	0.891	-1.378	-4.771
Priest Landing	1.305	0.109	0.943	-0.956	-3.997
Richmond Hill	1.686	0.392	0.892	-1.258	-4.069
Range A Light	1.500	0.129	0.942	-1.252	-4.557
Sunbury	1.407	0.115	0.945	-1.094	-4.244
Crispen Island	2.078	0.202	0.882	-2.637	-6.923
Dungeness	1.960	0.287	0.823	-2.366	-6.586

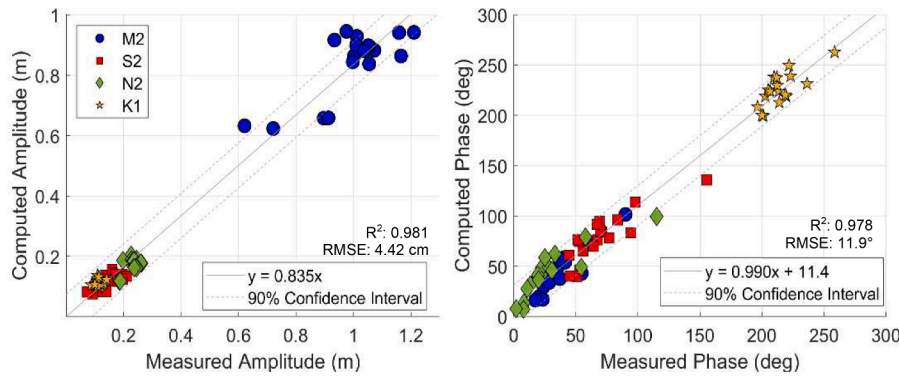


Fig. 5. Root mean squared error, MSE/VAR, correlation coefficient (R^2), relative bias, and scatter index between NOAA-observed and ADCIRC-simulated amplitude and phase for the M2, S2, N2, and K1 constituents for all stations.

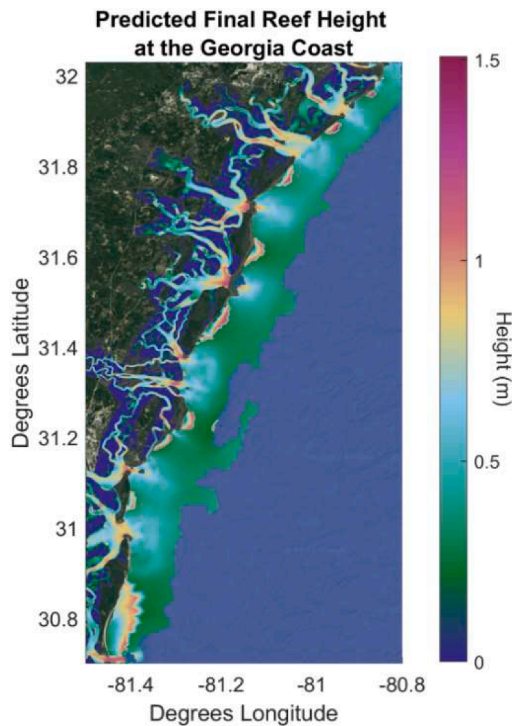


Fig. 6. Predicted final reef heights at the Georgia Coast.

Fig. 3 and information regarding each station is presented in Table 2.

The accuracy of the resynthesized water levels was assessed by calculating the root mean squared error (RMSE) (Eq. (15)) and the ratio of mean squared error (MSE) to population variance (VAR) (Eq. (16)), where M_t is the measured values, \bar{M}_t is the mean of the measured values, C_t is the computed values, and t is time.

$$RMSE = \sqrt{\frac{1}{N} \sum_t (M_t - C_t)^2} \quad (15)$$

$$\frac{MSE}{VAR} = \frac{\frac{1}{N} \sum_t (M_t - C_t)^2}{\frac{1}{N-1} \sum_t (M_t - \bar{M}_t)^2} \quad (16)$$

For water levels at the eighteen stations selected, the minimum and maximum RMSE were 0.708 cm and 2.078 cm, respectively. The highest errors were associated with stations located further upstream in reaches of tidal creeks, where there is insufficient availability of recent bathymetric data. The mean tidal range for the modeled water levels is 3.27 m and 2.46 m for the computed water levels. Normalized by the tidal

range, the maximum RMSE is less than 1 % of both the modeled and computed tide ranges and thus can be regarded as negligible. Similarly, the largest MSE/VAR was 0.392, observed at the Richmond Hill station. RMSE, MSE/VAR, correlation coefficient (R^2), relative bias, and scatter index values for all stations included in the resynthesis are presented in Table 3.

The ADCIRC simulation was further validated through comparison between the four dominant tidal constituents in the region (Fig. 5). For both amplitude and phase, the high correlation coefficient (0.981 and 0.977, respectively) indicates good agreement between measured and computed values. Similarly, the RMSE of modeled amplitude values versus observed was 1.138 cm. As the lower amplitude values were around 18 cm, an error of 1.138 cm can be considered negligible. In contrast, the lowest phase values within these four constituents were less than 1° , compared to the RMSE for phases being 3.23° , indicating greater error.

3.2. Oyster reef model

The HR16 + Hydro model predicts the final oyster, shell, and sediment layers. Reef height is equal to the sum of the oyster and shell layers if the sediment layer does not exceed the top of the oyster layer; otherwise, it is the sum of all three layers (Fig. 2). Generally, regions between tidal inlets and channel edges exhibit the highest predicted final oyster layer heights. Reefs adjacent to the coastline show an increase in height as the distance to the shoreline decreases (Fig. 6). The hydrodynamic conditions associated with these increases are characterized by greater depths and higher flow speeds, given the combination does not result in sediment deposition onto the reef. Reef height itself is primarily velocity limited, where the largest drivers of mortality are influenced by flow speed more than depth. In contrast, the reduction in breaking wave height by the reefs are depth limited rather than velocity limited, where the reduction of water column depth is directly related to the depth at which the reef is located.

The pronounced variations in oyster growth at small distances highlight the sensitivity of sediment deposition to velocity and depth (Fig. 7). This is due to an intermediate velocity threshold existing between ~ 0.8 and $\sim 1.8 \text{ m s}^{-1}$ where sediment begins to infiltrate the live oyster layer, resulting in a different behavior of the sediment regime (Eqs. (7) and (14)).

3.2.1. Spatial analysis of oyster growth

To evaluate the flow velocities and total water depths that yield the highest oyster layer and reef heights, heights were plotted against various hydrodynamic variables to examine how velocity and depth influence factors that contribute to either growth or mortality (Fig. 8). In all cases, the response of oyster layer height and total reef height falls into one of two regimes. The first regime (regime 1, or R1) is categorized as situations where sediment layer has not infiltrated the oyster layer,

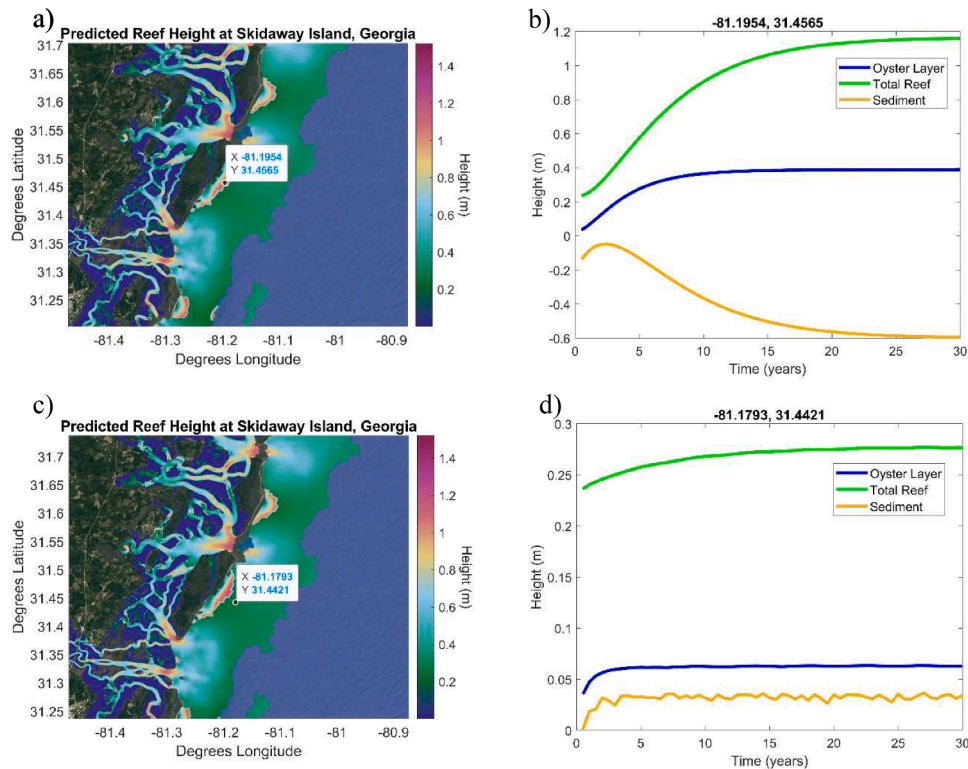


Fig. 7. Oyster layer height and sediment layer height time series at areas between tidal inlets along the Georgia coast. In a) areas of higher reef heights, the b) growth rate of the reef was able to surpass that of sediment deposition, reducing the mortality rate from sediment deposition. In contrast, c) areas where reefs performed relatively worse were associated with d) mortality rates greater than growth rates due to the deposition of sediment, reflecting the sensitivity of reefs to spatially varied physical constraints.

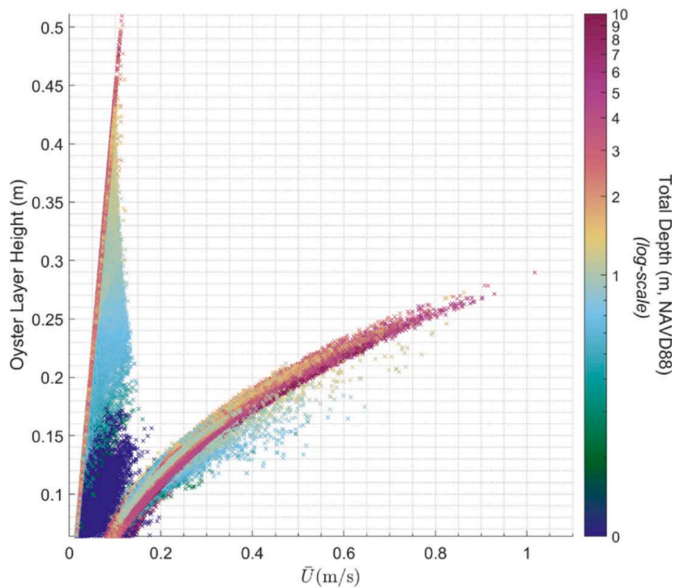


Fig. 8. Oyster layer height response to average velocity magnitude and total water depth after 30 years.

while the second regime (regime 2, or R2) is where the sediment layer has infiltrated the oyster layer, resulting in additional mortalities due to smothering by sediment. This distinction impacts the calculation of adjusted sediment concentration (Eq. (10)) and shear stress (Eq. (14)) equations that account for the relative position of the live oyster layer and sediment layer.

At year thirty, the highest oyster layer height is observed at velocities

of 0.115 m/s (Fig. 9). Velocities below this threshold are categorized under the first regime (R1). Oyster layer height increases linearly with depth until reaching approximately 1.7 m, where the overall highest oyster layer height is observed at a 1.86 m depth and a 0.115 m/s flow speed. Beyond this velocity (R2), oyster layer height is reduced to less than 10 cm but continues to increase with velocity, albeit at a smaller growth rate. Starting at 0.08 m/s, oyster layer height increases logarithmically with velocity, with lower final reef heights observed at smaller depths coupled with lower velocities.

The change in oyster growth rates in response to velocity is attributed to the transition from a sediment-free oyster layer to the onset of smothering by sediment deposition (Fig. 10). After this transition, the growth and mortality terms begin to account for smothering by sediment, where growth is limited to the fraction of oysters free from sediment and mortality increasing at the same magnitude as the reduced growth rate.

3.2.2. Analysis of reef compositions

As the simulation progresses, the percentage of the total reef height composed of dead shell approaches two values: approximately 66 % in regime 1 and 78 % in regime 2 (Fig. 11). At the thirty-year timestep, the values associated with higher velocities are still approaching 66 % and may reach equilibrium values beyond 30 years. At depths greater than 1 m, oyster layer height and the percentage of reef that is composed of shell follow a closely related exponential decay pattern, with greater deviation observed at lower depths and a slower rate of convergence to these values.

The two equilibrium values are analogous to the change in growth rate when sediment infiltrates the oyster layer. Because the equations for the sediment layer change when this condition is met, both the growth and the mortality terms of the oyster layer equation become dependent upon the fraction of the oyster layer covered by sediment. As a result, the

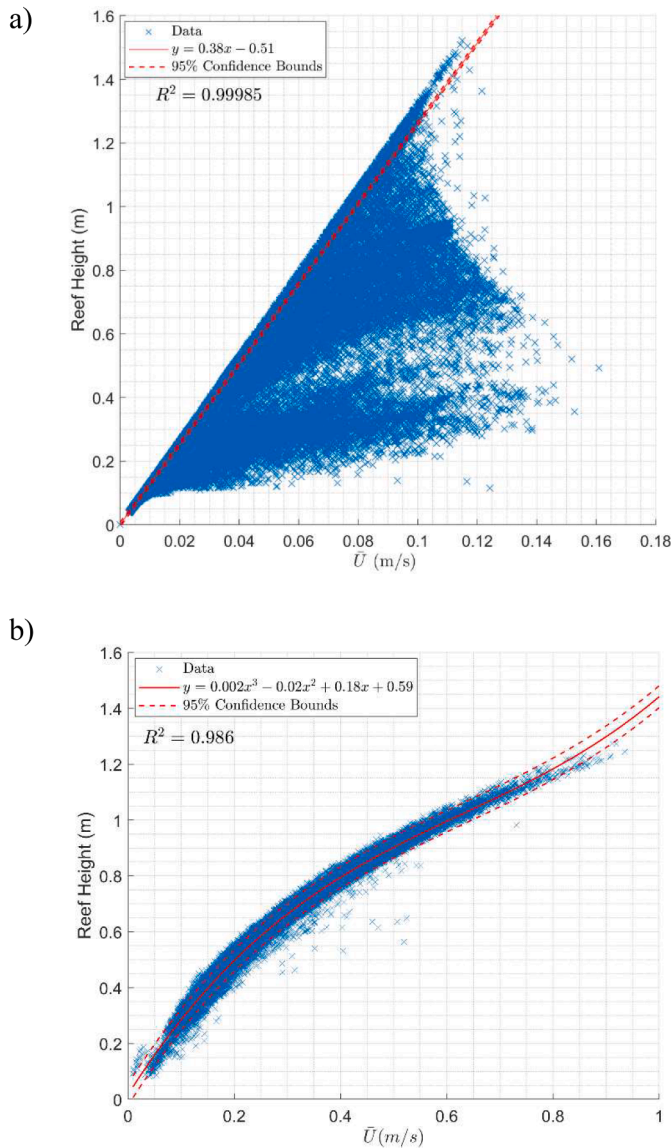


Fig. 9. Reef height to average velocity magnitude a) in the absence of sediment (R1) and b) when sediment produces additional mortalities (R2).

mortality rate increases while the growth rate decreases, subsequently increasing the shell layer to oyster layer ratio.

3.3. Application in design of nature-based solutions

Wave breaking is depth-limited (Kamphuis, 2020), and the final reef height determines the percentage of the water column occupied by the reef. This, in turn, affects the reduction in breaking wave height (Fig. 12). Breaking wave height, H_b , is often computed as:

$$H_b = \gamma h_b \tag{17}$$

where h_b is the depth of the water column at the point of breaking times and γ is the breaker index (~ 0.78) (McCowan, 1894). The reduction in water column height due to the presence of the reef structure reduces the likelihood of wave heights exceeding the waveheight/wavelength ratio required for breaking ($1/7$) (Webb, 2017), the breaking wave height itself, and the likelihood of waves propagating further inland.

The greatest reduction in wave breaking height, and thus the greatest potential to dissipate wave energy (Kamphuis, 2020), occurs in regions between tidal inlets and along the edges of channels. These areas are

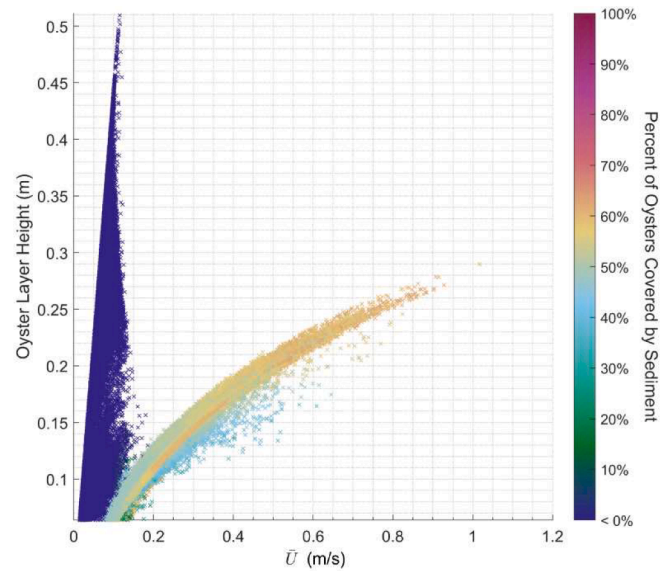


Fig. 10. Oyster layer height response to sediment deposition after thirty years. Second regime exhibits smaller final reef heights.

associated with greater final reef heights. However, as the degree of wave height reduction depends on the reef's height relative to the water column depth, reduction in wave heights are observed in areas where the oyster reef is relatively shorter as well.

Unlike the reef height itself, reduction in breaking wave height is depth limited rather than velocity limited. This is evident by water column height reductions consistently reaching as high as 50 % for all velocities greater than 1 cm/s, despite lower reef heights after $\sim 0.8\text{--}0.18$ m/s (Fig. 13). This suggests that it is possible to incorporate oyster reef living shorelines as a nature-based solution without the requirement of maximum oyster growth. Instead, a sufficient growth rate is necessary for the population to persist and supply the mortality needed to maintain the shell layer.

4. Discussion

4.1. Wave attenuation by predicted oyster reefs

To assess the ability of the predicted oyster reefs within the South Atlantic Bight to provide shoreline protection, the final reef heights associated with each node and their reduction in bathymetry were used in several ADCIRC + SWAN simulations. The SWAN (Simulating WAVes Nearshore) model, coupled with ADCIRC, incorporated storm surge and wave generation as well as dissipation (Dietrich et al., 2012) in several synthetic storm simulations. The SWAN component of the model uses the same unstructured mesh as the previous ADCIRC simulations.

The synthetic storms included in these simulations belong to a collection of 1060 tropical synthetic storms developed by the U.S. Army Corps of Engineers Coastal Hazards System (CHS) South Atlantic Coastal Study (Nadal-Caraballo et al., 2020) (<https://chs.ercd.dren.mil/>). Eight storms were selected to assess the performance of oyster reef breakwaters along Coastal Georgia (Fig. 14). The chosen storms exhibit variation in parameters such as track angle with respect to north (θ), central pressure deficit (∂P), radius to maximum wind speeds (r_{max}), velocity of the storm (v_f), and maximum wind speeds v_{wind} . This range in parameters enables the assessment how oyster reefs attenuate waves across different storm intensities and angle of approach towards the shoreline (Table 4).

Two simulations were conducted per storm, where all inputs and parameters other than bathymetry were identical. The first simulation was performed with the original bathymetry, thereby not considering

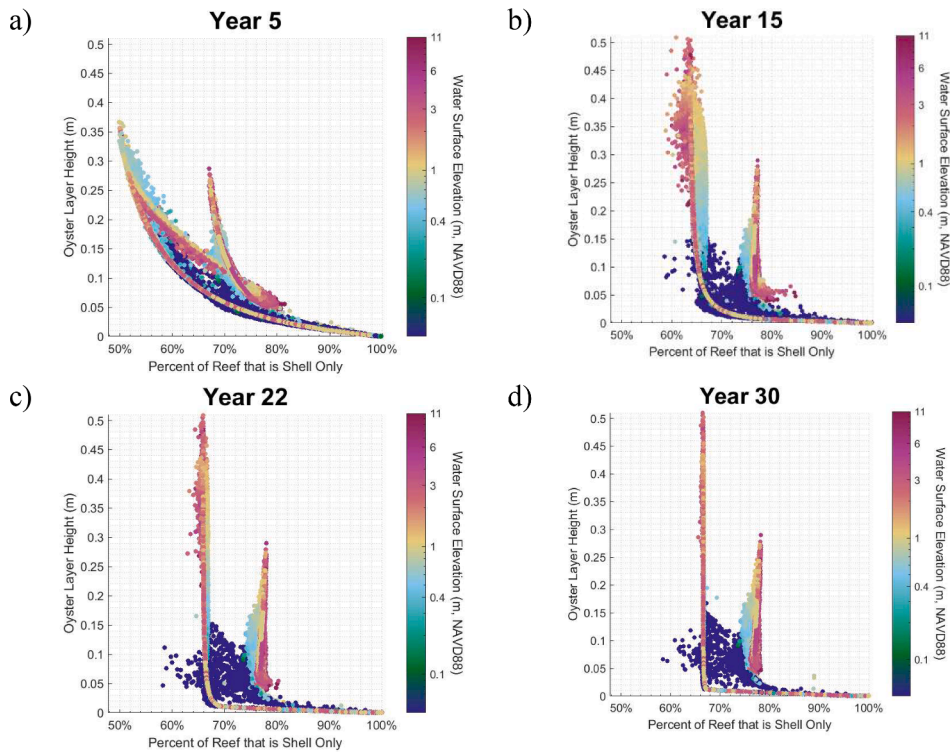


Fig. 11. Temporal analysis of percent of reef height that is composed of dead shells in response to mean sea level at a) year 5, b) year 15, c) year 22, and d) year 30.

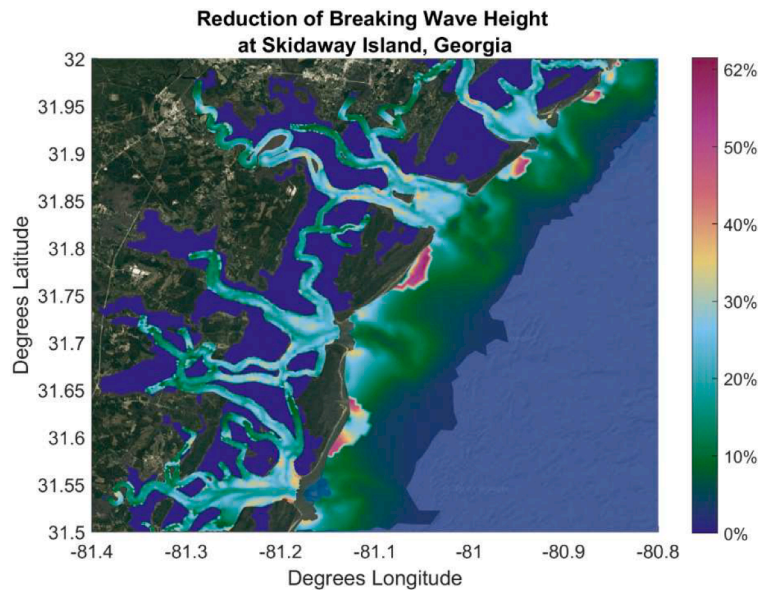


Fig. 12. Reduction of breaking wave height at Skidaway Island, Georgia.

the presence of oyster reefs. The second simulation accounted for reduced total water level caused by the presence of reefs in the water column, resulting in new bathymetry within the mesh. Both maximum water surface elevations and significant wave heights for each node were computed for both simulation scenarios

The different node elevations were compared to assess the change in storm-related hydrodynamic impacts when oyster reef breakwaters are deployed. A reduction in maximum significant wave height is observed for all storms irrespective of their intensity or approach angle to the shore (Fig. 15). Due to counterclockwise wind rotation, the greatest wave attenuation is concentrated north of each storm track for most

storms, excluding storms whose tracks are close to shore-parallel at small distances from the coast. This may suggest that oyster reefs present greater performance as wind waves approach perpendicular to the shoreline. While the reefs at their predicted elevations were observed to reduce maximum significant wave heights across all storms, it is important to note that oyster reefs do not necessarily reduce total water levels. The vertical relief of oyster reefs has been found to attenuate waves with heights less than double the reef height (Chowdhury et al., 2019), but does not block flow entirely unless the water depth is less than that of the reef. As such, the dissipation of wave energy and wave breaking produced by reefs reduces wave heights as opposed to the total

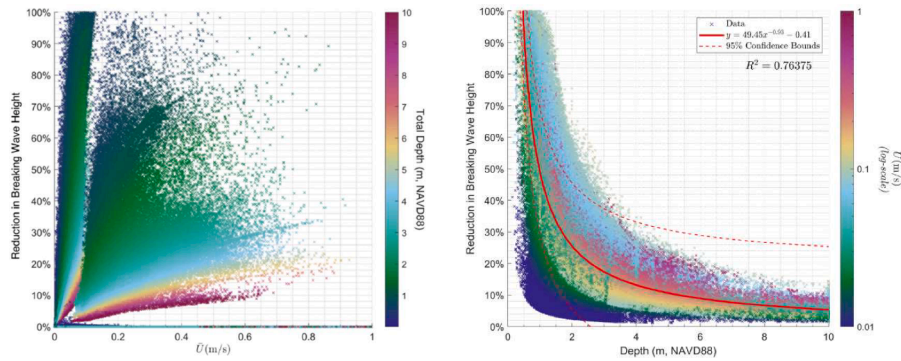


Fig. 13. Reduction in breaking wave height by reef in response to average a) velocity magnitude and b) total water depth.

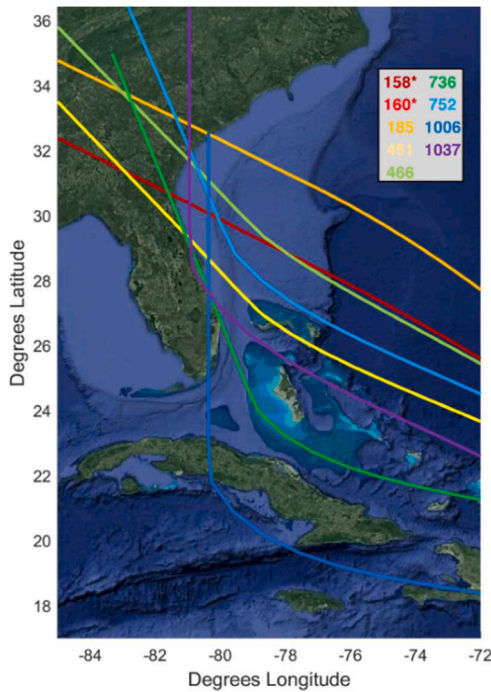


Fig. 14. Tracks of synthetic storms selected for simulation. *Storms 158 and 160 have identical storm tracks but differ in intensity.

Table 4
Parameters for each synthetic storm. Maximum wind speed for each storm is the maximum observed within the South Atlantic Bight.

Storm ID	θ (deg)	∂P (hPa)	r_{max} (km)	v_f (km/h)	$v_{w,max}$ (mph)
158	-60°	48	26	22.3	77.93
160	-60°	8	120.3	17.6	27.72
185	-60°	148	34.8	9.8	155.2
451	-40°	18	56.5	18.5	53.32
466	-40°	138	43	9.7	120.5
736	-20°	8	142.3	22.4	29.01
752	-20°	8	82.9	30.9	37.89
1006	0°	118	10.1	15.2	157.6
1037	0°	58	18.7	14.4	86.02

water level at depths greater than the reef height (Fig. 16).

While several studies highlight the promising ability of oyster reefs to protect shorelines (Chauvin, 2018; Chowdhury et al., 2019; Scyphers et al., 2011; Wiberg et al., 2018), there is a lack of evidence supporting the success of both ecological and engineering performance in oyster

reef breakwaters simultaneously. Morris et al. (2021) found that environments conducive to oyster reef growth were associated with minimal added wave attenuation enhancements, whereas areas in which reefs were likely to provide greater attenuation were associated with a more unfavorable habitat. Prior studies found wave attenuation to be significant when the reef elevation meets or surpasses the water level (Chauvin, 2018; Wiberg et al., 2018), but is associated with lower reef heights. The predicted final reef heights in our oyster reef model suggest the greatest reduction in water levels are consistent with these studies, given that the highest final reef heights are positioned at greater depths. As a result, when designing for shoreline defense, consideration for locations that are likely to result in a greater proportion of the water column being occupied should supersede that which prioritizes overall reef growth alone.

The results of the simulations operate on the assumption that reef exists at each node predicted by the oyster reef model. As a result, there is difficulty in attributing changes in hydrodynamics observed in the model to a particular reef location. Changes in radiation stress gradients produced by reef breakwaters were seen across large spatial scales and may suggest resulting flow impacts on surrounding areas when a reef is isolated. However, these impacts were not reflected in the storm simulation results but should be considered in future model developments. Moreover, isolating reefs to small areas of interest presents an opportunity for improved validation and utility as a tool for designing oyster reef breakwaters. Nevertheless, as a first-pass simulation, the model results indicated that oyster reefs reduce significant wave heights during storm events at depths consistent with prior studies.

4.2. Model sensitivity

The sediment layer height was observed to increase with velocity, which was initially counter-intuitive. The sediment deposition term (Eq. (6)) hinges on both depth and velocity. Before reaching a critical flow speed, sediment deposition isn't substantial enough to elevate the sediment layer above the shell layer. The deposition rate does not outpace the growth rate which increases due to the greater vertical mixing of food particles triggered by higher flow speeds (Housego and Rosman, 2016).

However, as sediment concentration above the reef (C) increases exponentially, which occurs when the sediment layer reaches the oyster layer, increased mortality due to smothering by sediment and stunted growth rates ensue. After this point, an increase in velocity results in taller oyster layers. This is partially due to sediment motion induced by adequate shear stress, which erodes sediment from the reef, and the augmented transport of food throughout the water column resulting from the same. This was also observed in the original HR16 model during their analysis of final reef height on flow speed (Housego and Rosman, 2016). It is known that oysters are sensitive to sediment deposition (Colden and Lipcius, 2015; Jordan-Coolley et al., 2011; Powers et al., 2009; Rose, 1973), but quantification of sediment-induced

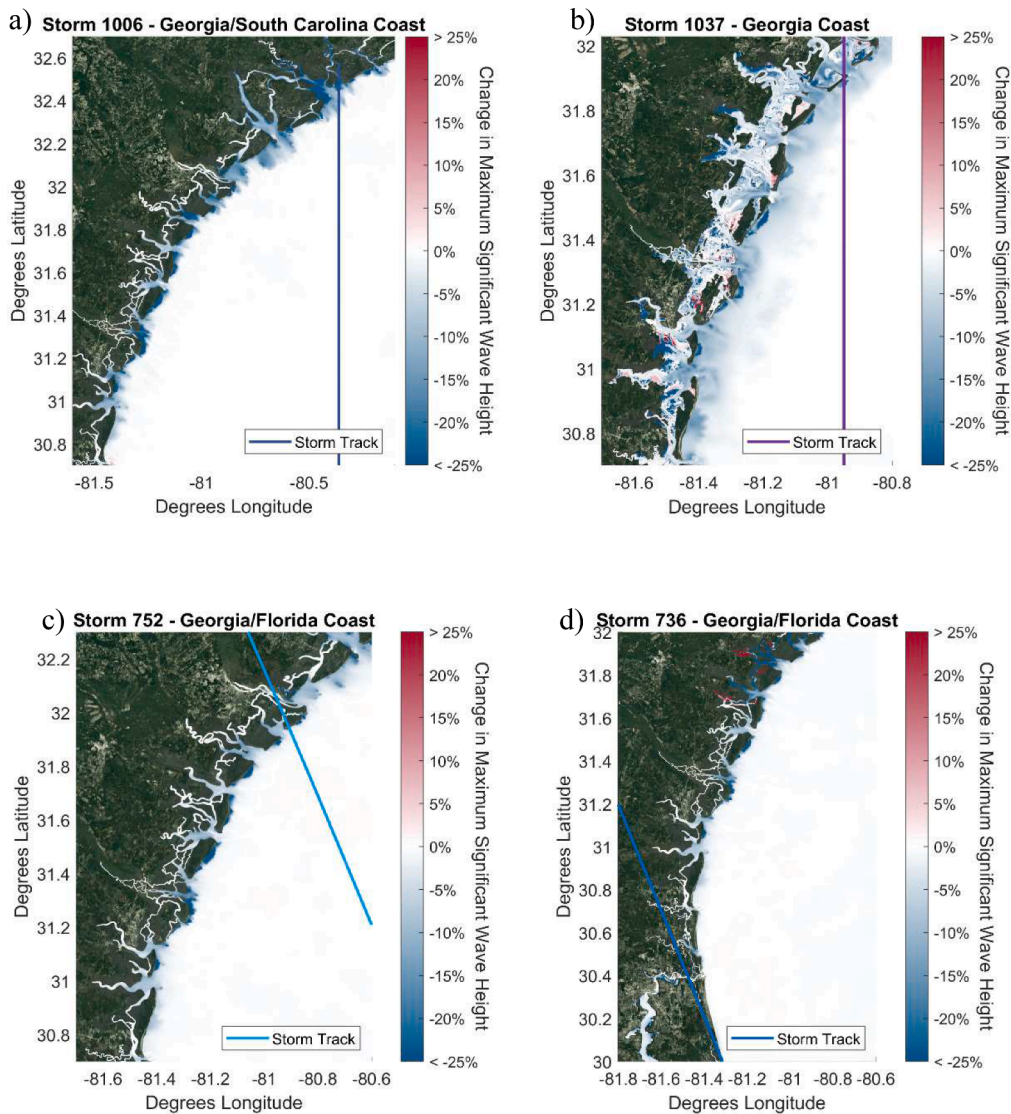


Fig. 15. Change in significant wave height resulting from the presence of the predicted final oyster reef heights across storms with ranging maximum wind speeds and angle of approach with respect to the shoreline. The wind speed for storms a) 1006, b) 1037, c) 752, d) 736 are 158 mph, 86 mph, 37.9 mph, and 29 mph, respectively.

mortality varies with hydrologic regime.

Greater sediment concentrations at higher velocities are a characteristic of the Rouse sediment concentration profile (van Rijn, 1993). Here, the deposition process is influenced by the suspended sediment's elevation and quantity within the water column rather than the settling velocity (Fig. 17). Consequently, increased velocities lift sediment higher in the water column and enhance the deposition potential onto the reef.

To determine when the sediment layer height reaches the oyster layer, a separate simulation, independent of ADCIRC, was conducted where depth was varied from 0 to 11 m and velocity was varied from 0.05 to 1 m/s, with a timestep of 0.1 years. The depth, velocity, and timestep combination was recorded when the sediment layer height exceeded the shell layer height. The results of this simulation suggest that regime changes within the first five years occur at 0.125 m/s when depths are greater than 6 m, with the velocity threshold increasing exponentially with decreasing depths (Table 5). The time at which the sediment layer reaches the oyster layer is indicative of the moment at which the rate of sediment deposition has outpaced the growth rate of the oysters. For each depth, increasing the velocity past the initial threshold value results in the regime change occurring at a later time,

indicating a higher ratio of growth rate to deposition rate (Fig. 18).

4.2.1. Sediment grain size

Sediment deposition and erosion are both functions of grain size d . The model assumes a constant grain size of 0.1 mm, consistent with that of the HR16 model. A separate, smaller scale simulation was conducted to evaluate whether variations of grain size influence model predictions. In this simulation, depth and velocity were assumed to be 3 m and 0.1 m/s, respectively, to ensure that grain size is the only parameter influencing results. Grain size was varied between a minimum mud grain size value, 0.001 mm (Wentworth, 1922) and maximum sand grain size value of 2 mm (Peralta et al., 2000).

Grain size, oyster layer height, and fraction of oysters occupied by sediment were plotted to evaluate the response of sediment deposition. Across the range of grain sizes, oyster layer height remained largely unaffected by increased sediment diameter, with the notable exception of diameters within the 0.012–0.019 mm range.

Within this range, sediment deposition is observed to reach a value substantial enough to infiltrate the oyster layer, consequently causing additional mortalities. Deposition within this range displayed a Gaussian distribution with a peak at approximately 0.05 mm.

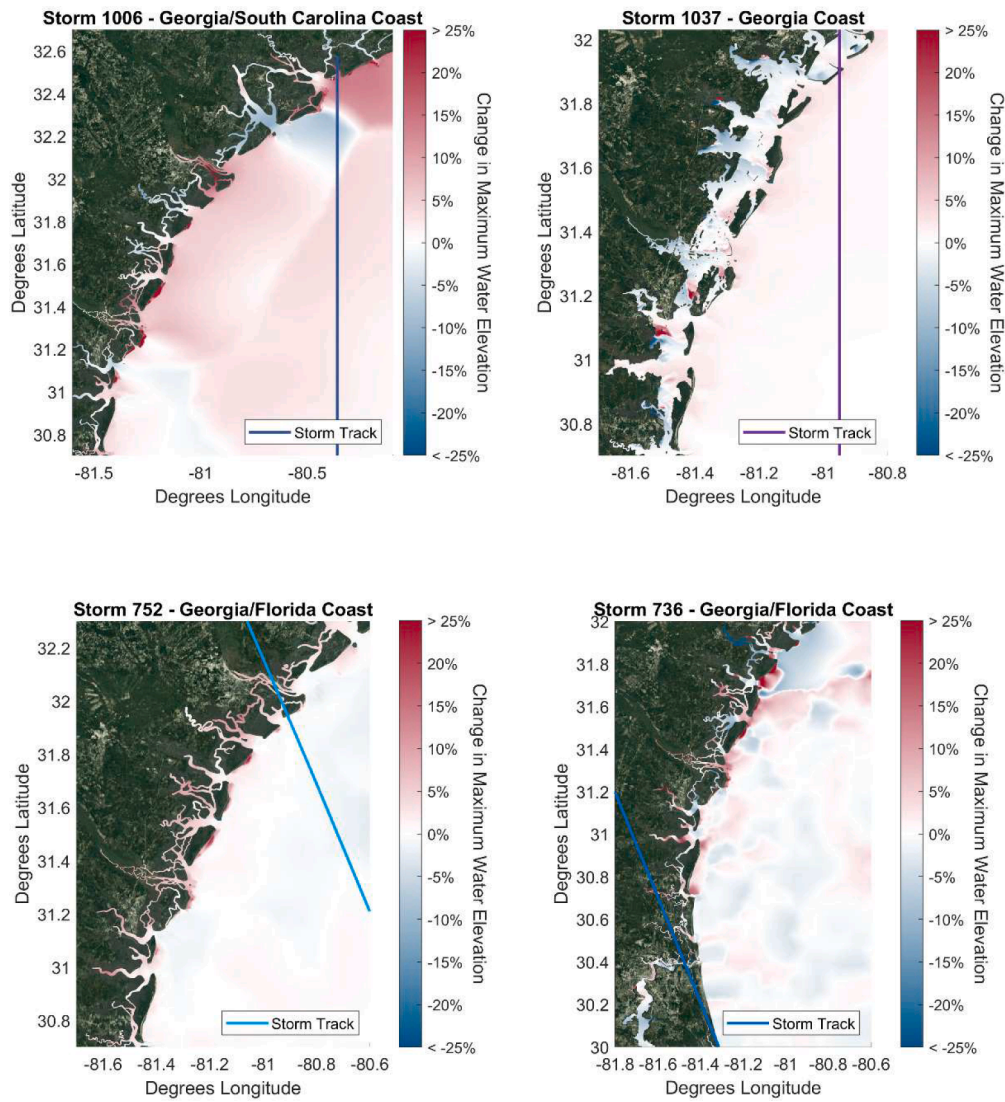


Fig. 16. Change in maximum water elevation resulting from the presence of the predicted final oyster reef heights across storms with ranging maximum wind speeds and angle of approach with respect to the shoreline. The wind speed for storms a) 1006, b) 1037, c) 752, d) 736 are 158 mph, 86 mph, 37.9 mph, and 29 mph, respectively.

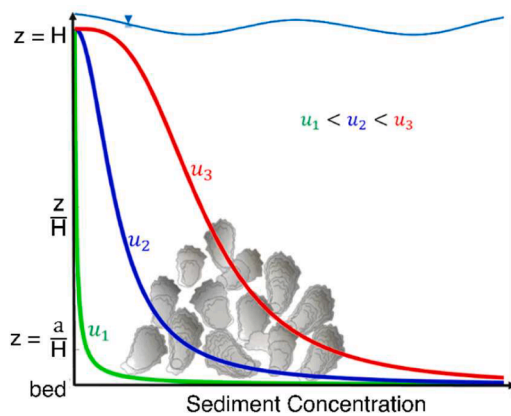


Fig. 17. Interaction between van Rijn concentration profile and increasing velocity. z is elevation above the bed, H is the total water column depth, and u is the flow speed.

Deposition, as calculated by the product of sediment concentration above the reef C (Eq. (8)) and the settling velocity W_s (Eq. (9)) also depends on the reef height, and the calculation for C depends on

whether the sediment layer has covered the top of the reef. As W_s is present the numerator and the integrated denominator of C , it can be hypothesized that this behavior is restricted to the observed range due to complex dynamics and result from specific numerical combinations of reef height and grain size values of which results in $C_{s,a}$ being small enough to increase C .

Similarly, shear stress, τ_b , is also unaffected by grain sizes beyond the range observed. Like deposition, the calculation of τ_b depends on the current categorization of the reef structure regime. While d is not present in the shear stress equation (Eq. (14)), τ_b is calculated based on the relative layer heights of the reef and therefore responds to the relative sediment layer height which is determined by the deposition observed in previous timesteps.

For sediment motion to be induced, the shields parameter θ must reach the critical shields value θ_c of 0.05. θ is a function of both τ_b and d itself. Within the grain size range that results in deposition, there exists a sufficient shear stress and an optimal grain size where θ is above threshold for erosion to occur (Fig. 19).

The oyster layer height was observed to exhibit fluctuations as the grain size incrementally increased within the specified range, where erosion is greater than erosion at certain diameters, until a slightly larger

Table 5
Minimum velocity for change in regime at varying depths.

Depth (m)	0.5	1	2	3	4	5	6	7	8	9	10	11
Velocity (m/s)	0.220	0.160	0.140	0.130	0.130	0.130	0.125	0.125	0.125	0.125	0.125	0.125

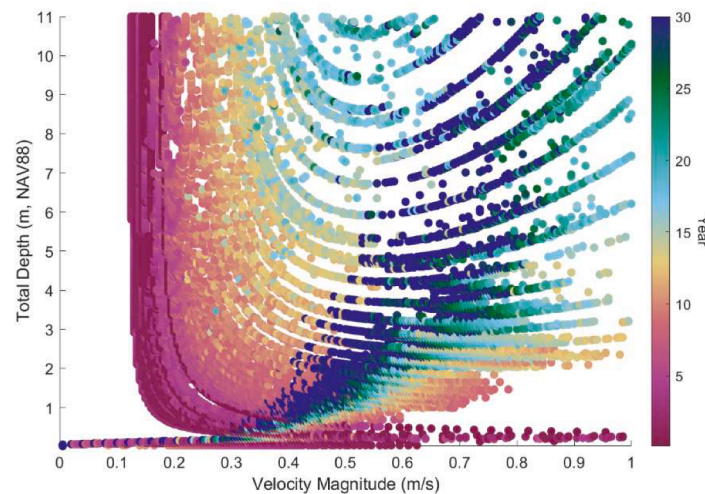


Fig. 18. Variation in regime change with total depth, velocity magnitude, and time.

size threshold is met, resulting in deposition overtaking erosion. Because erosion increases with greater sediment amount within the reef, states of greater erosion and greater deposition alternate as the simulation progresses (Fig. 20).

Nevertheless, it can be concluded that grain size does not influence model results if the observed grain size does not fall within this range. It should be noted that the range at which this behavior occurs also depends on depth and velocity but can be determined on a case-by-case basis. Furthermore, this behavior is observed only with very small grain sizes.

4.3. Limitations and future work

This study only considered depths less than 11 m and found that oyster layer height did not exhibit significant variation with water depth, consistent with previous studies measuring depth of inundation (Byers et al., 2015), but showed lower final reef heights when more time was spent emerged from water. Generalizing these patterns may be difficult, as an oyster's elevation on the reef, which has been shown to have a significant influence on growth (Bartol et al., 1999), is not accounted for in the model. Elevation of live oysters on the reef is assumed to have no effect on the depth and flow velocity – the live oyster layer, in the model, will experience the same sedimentation, erosion, and other effects. The elevation of oysters on the reef regulates the impact of dissolved oxygen and predatory pressure, where oysters growing near the bottom face disadvantages (Campbell and Hall, 2019; Lenihan et al., 2001). On the other hand, higher elevations on the reef can result in drying out and lower food availability (Michener and Kenny, 1991; Kingsley-Smith and Luckenbach, 2008).

Moreover, the position and orientation of oysters on the reef were not considered. Studies have found oyster shell reefs perpendicular to flow promote reef persistence (Colden et al., 2016), and higher growth and lower mortality rates occur on reef crests where flow velocity is higher (Lenihan, 1999). Future adaptations of the model should simulate depth and changing velocity throughout the water column by individual oysters rather than the oyster layer. The former is accounted for in the model in that oysters are unable to grow if exposed during low tide

but are still able to grow at high tide.

The model's assumption of constant grain size neglects turbulence variance with substrate material or bed material, creating inaccuracies in flow simulations. As such, validation requires field experiments assuming the same sediment properties as the model (Grizzle et al., 1992). While additional analysis found that grain size does not pose a significant influence on model results, including spatially varied sediment composition and grain size using USGS data (U.S. Geological Survey, 2020) could account for land subsidence by factoring in reef weight and bed sediment composition and properties. However, because the reefs in this model are assumed to be those constructed in a living shoreline application, the substrate material of the bed is not influential to the ability of other oysters to settle.

Recruitment success, reproduction rates, and disease susceptibility are greatly influenced by biophysical parameters like temperature and salinity (Bartol and Mann, 1997; Ford et al., 2012; Hofmann et al., 2001; Munroe et al., 2015; Powell et al., 2012). However, the purpose of this model is to isolate the role of hydrodynamics in influencing oyster reef growth and thus assumes all other biological needs are met. As such, salinity is not included in the model, and temperature is assumed to be a fixed value, limiting this study to geophysical impacts on reef growth. While absolute reef height does vary with temperature, the spatial distribution of taller reefs does not change. As a result, the model is still effective at assessing hydrodynamic conditions alone. Regardless, classifying a site as a suitable habitat requires further investigation with attention to both biophysical and ecological processes, and thus temperature should be considered in future analyses. The HR16 model structures growth to include temperature (albeit constant), enabling integration of spatially or temporally varying temperature models. This expansion could determine the response to warming oceans due to climate change.

Furthermore, validation of model results is limited by the availability of data in the literature. Field measurements of oyster growth show considerable variation (Harsh et al., 1995) likely due to heterogeneity of surface roughness and turbulence in flows. Lenihan et al. (1996) found oysters have higher growth rates with increasing velocities, with a maximum growth at velocities of 0.07 m/s (the highest flow speed

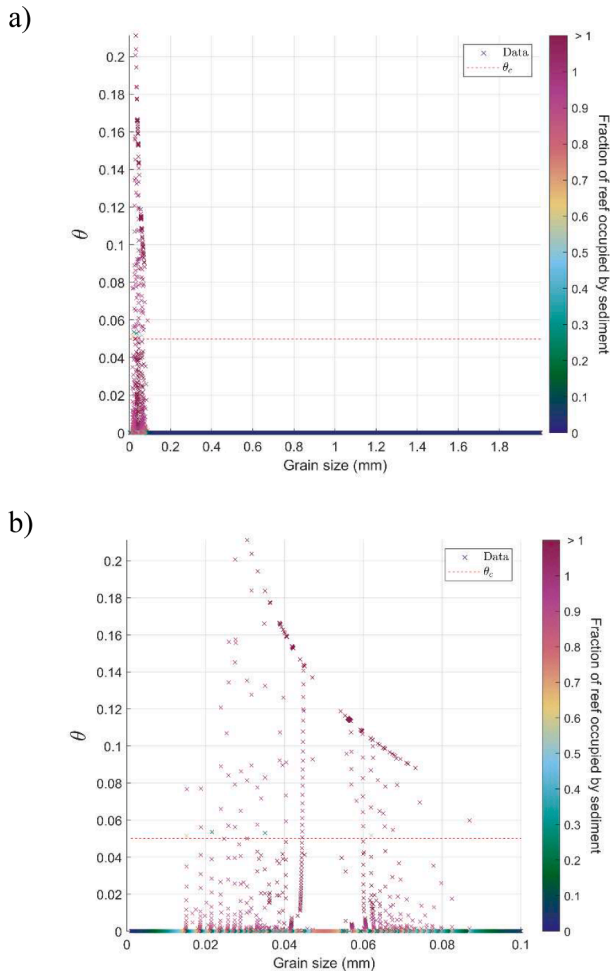


Fig. 19. a) Shields parameter across all grain sizes evaluated and b) the shields parameter within the range producing sediment infiltration.

measured in the study), while other studies (Grizzle et al., 1992) observed increased growth with increasing velocities, but with growth peaking at 0.01 m/s and declining with further increasing speeds.

Although the latter study’s maximum growth is an order of magnitude smaller than the model’s mid-range, model results indicate a range of velocities producing peak (and decline immediately following) growth rates that are dependent upon depth as well as the dynamic of growth rate and sediment deposition rate, and can be attributed to variation in both as well as initial layer heights (Housego and Rosman, 2016). Because variation of biological parameters is neglected, field-based data of biological metrics should be collected and used in a model simulation for validation in future efforts.

5. Conclusions

Oyster reefs can serve as natural breakwaters (Meyer et al., 1997) and therefore are a promising option for shoreline defense. However, successful implementation of oyster reefs a nature-based solution requires meeting their survival needs (Morris et al., 2019). Modeling environmental conditions promoting successful reef growth can predict optimal areas for implementing reefs as a form of shoreline protection (Fuchs and Reidenbach, 2013; La Peyre et al., 2015). This model links an existing point-based model to a hydrodynamic model (ADCIRC) to predict the locations and associated hydrodynamic conditions of tallest final reef heights.

Generally, the simulation predicts the tallest final reef heights near the shore between tidal inlets, at shallower depths of tidal inlets, and at tributary edges. While oysters are generally not found in tidal inlets, these locations serve as predictions on a first-pass, physical basis only, not accounting for extraneous factors like ecology, human influence, harvesting, or land subsidence. Nevertheless, analysis of oyster layer height and total reef height response to depth and velocity reflected a transition in behavior when sediment enters the oyster layer. Before this threshold, final oyster layer heights increase linearly with velocity, with the critical velocity at which the regime change occurs varying with depth and the time when the deposition rate outpaces the growth rate, ranging from 0.08 m/s to 0.18 m/s. Greater depths experience a regime change at the lower end of this range, and vice versa.

The greatest potential for application as living shorelines, measured by the greatest percentage of the water column occupied by the reef and the subsequent reduction in significant wave height, lies where depths are less than 3 m, or where reefs occupy more than fifty percent of the water column. This occurs nearshore and close to the coastline but

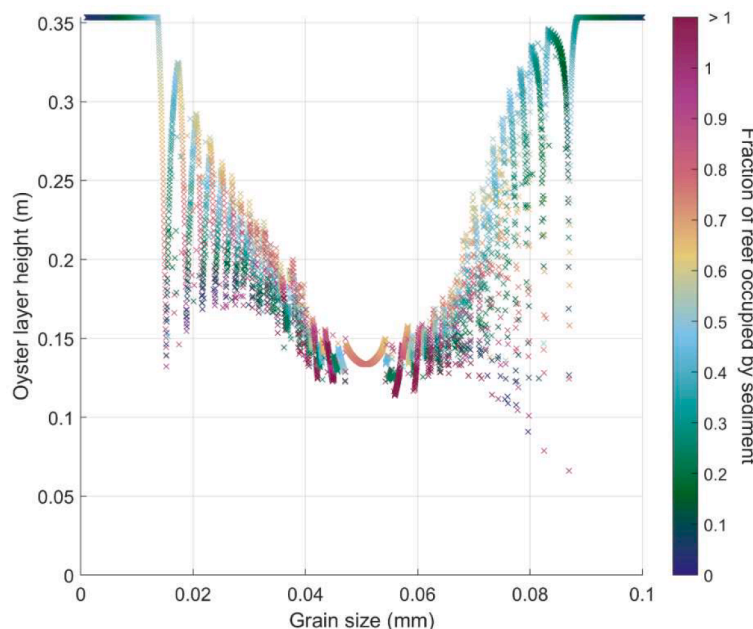


Fig. 20. Fluctuation in removal and deposition of sediment with varying grain size.

includes additional locations without high predicted final oyster layer heights. The increased range is attributed to the remaining shell layer during mortality, where the oyster layer growth rate sufficiently supports the oyster population that perishes and adds to the shell layer without population collapse.

Although the model does not account for additional mortality or population decline contributors that may cause inaccuracies in predictions, incorporating spatially varying hydrodynamic variables lays the foundation for further adjustments, adaptations, and expansions. Future contributions to this model's development will enhance its utility as a tool for designing nature-based infrastructure.

CRedit authorship contribution statement

Rebecca E. Stanley: Writing – original draft, Writing – review & editing, Conceptualization, Methodology. **Matthew V. Bilskie:** Writing – review & editing, Conceptualization, Methodology, Supervision. **C. Brock Woodson:** Writing – review & editing. **James E. Byers:** Writing – review & editing, Conceptualization, Methodology, Supervision.

Declaration of competing interest

The authors declare that they have no known competing financial interests or personal relationships that could have appeared to influence the work reported in this paper.

Data availability

Data will be made available on request.

Acknowledgment

This study was conducted as part of a Network for Engineering With Nature (N-EWN) collaborative research effort between the University of Georgia and the U.S. Army Corps of Engineers' Research and Development Center (ERDC) Award W912HZ2020031.

References

- Adams, M.P., Walker, R.L., Heffernan, P.B., 1995. The effects of stocking density, bag mesh size, and bottom sediment on the growth and survival of the eastern oyster, *Crassostrea virginica*, with emphasis on controlling oyster spat fouling. *J. Appl. Aquac.* 4 (4), 25–44. https://doi.org/10.1300/J028v04n04_03.
- Aguilera, M.A., Arias, R.M., Manzur, T., 2019. Mapping microhabitat thermal patterns in artificial breakwaters: alteration of intertidal biodiversity by higher rock temperature. *Ecol. Evol.* 9 (22), 12915–12927. <https://doi.org/10.1002/ece3.5776>.
- Atkinson, L.P., Menzel, D.W., Bush, K.A., 1985. Oceanography of the Southeastern U.S. Continental Shelf, 2. American Geophysical Union. [10.1029/CO002](https://doi.org/10.1029/CO002).
- Bacopoulos, P., Hagen, S.C., 2017. The intertidal zones of the South Atlantic Bight and their local and regional influence on astronomical tides. *Ocean. Model.* (Oxf) 119, 13–34. <https://doi.org/10.1016/j.ocemod.2017.09.002>.
- Bacopoulos, P., Parrish, D.M., Hagen, S.C., 2011. Unstructured mesh assessment for tidal model of the South Atlantic Bight and its estuaries. *J. Hydraul. Res.* 49 (4), 487–502. <https://doi.org/10.1080/00221686.2011.552465>.
- Bahr, L.M., Lanier, W.P., 1981. The Ecology of Intertidal Oyster Reefs of the South Atlantic Coast: a Community Profile. FWS/OBS.
- Bartol, I.K., Mann, R., 1997. Small-scale settlement patterns of the oyster *Crassostrea virginica* on a constructed intertidal reef. *Bull. Mar. Sci.* 61 (3), 881–897.
- Bartol, I.K., Mann, R., Luckenbach, M., 1999. Growth and mortality of oysters (*Crassostrea virginica*) on constructed intertidal reefs: effects of tidal height and substrate level. *J. Exp. Mar. Biol. Ecol.* 237 (2), 157–184. [https://doi.org/10.1016/S0022-0981\(98\)00175-0](https://doi.org/10.1016/S0022-0981(98)00175-0).
- Blanton, B.O., Werner, F.E., Seim, H.E., Luettich, R.A., Lynch, D.R., Smith, K.W., Voulgaris, G., Bingham, F.M., Way, F., 2004. Barotropic tides in the South Atlantic Bight. *J. Geophys. Res.* 109 (12), 1–17. <https://doi.org/10.1029/2004JC002455>.
- Bouma, T.J., van Belzen, J., Balke, T., Zhu, Z., Airolidi, L., Blight, A.J., Davies, A.J., Galvan, C., Hawkins, S.J., Hoggart, S.P.G., Lara, J.L., Losada, L.J., Maza, M., Ondiviela, B., Skov, M.W., Strain, E.M., Thompson, R.C., Yang, S., Zanuttigh, B., Herman, P.M.J., 2014. Identifying knowledge gaps hampering application of intertidal habitats in coastal protection: opportunities & steps to take. *Coast. Eng.* 87, 147–157. <https://doi.org/10.1016/j.coastaleng.2013.11.014>.
- Breitburg, D., 1999. Are three-dimensional structure and healthy oyster populations the keys to an ecologically interesting and important fish community? In: Bilkovic, D.M., Mitchell, M.M., La Peyre, M.K., Toft, J.D. (Eds.), Luckenbach MW, Mann R, Wesson JA Oyster Reef Habitat Restoration: A Synopsis and Synthesis of Approaches, pp. 239–249.
- Breitburg, D.L., Palmer, M.A., Loher, T., 1995. Larval distributions and the spatial patterns of settlement of an oyster reef fish: responses to flow and structure. *Mar. Ecol. Prog. Ser.* 125 (1–3), 45–60. <https://doi.org/10.3354/meps125045>.
- Byers, J.E., Grabowski, J.H., Piehler, M.F., Hughes, A.R., Weiskel, H.W., Malek, J.C., Kimbro, D.L., 2015. Geographic variation in intertidal oyster reef properties and the influence of tidal prism. *Limnol. Oceanogr.* 60 (3), 1051–1063. <https://doi.org/10.1002/lno.10073>.
- Byers, J.E., Holmes, Z.C., Malek, J.C., 2017. Contrasting complexity of adjacent habitats influences the strength of cascading predatory effects. *Oecologia* 185 (1), 107–117. <https://doi.org/10.1007/s00442-017-3928-y>.
- Campbell, M.D., Hall, S.G., 2019. Hydrodynamic effects on oyster aquaculture systems: a review. *Rev. Aquac.* 11 (3), 896–906. <https://doi.org/10.1111/raq.12271>.
- Chauvin, J., 2018. Wave attenuation by constructed oyster reef breakwaters. LSU Master's Theses. https://digitalcommons.lsu.edu/gradschool_theses/4752.
- Chowdhury, M.S.N., Walles, B., Sharifuzzaman, S., Shahadat Hossain, M., Ysebaert, T., Smaal, A.C., 2019. Oyster breakwater reefs promote adjacent mudflat stability and salt marsh growth in a monsoon dominated subtropical coast. In: *Sci. Rep.*, 9. <https://doi.org/10.1038/s41598-019-44925-6>.
- Colden, A.M., Fall, K.A., Cartwright, G.M., Friedrichs, C.T., 2016. Sediment suspension and deposition across restored oyster reefs of varying orientation to flow: implications for restoration. *Estuaries Coast.* 39 (5), 1435–1448. <https://doi.org/10.1007/s12237-016-0096-y>.
- Colden, A.M., Lipcius, R.N., 2015. Lethal and sublethal effects of sediment burial on the eastern oyster *Crassostrea virginica*. *Mar. Ecol. Prog. Ser.* 527, 105–117. <https://doi.org/10.3354/meps11244>.
- Davis, J.L., Currin, C.A., O'Brien, C., Raffenburg, C., Davis, A., 2015. Living shorelines: coastal resilience with a blue carbon benefit. *PLoS ONE* 10 (11). <https://doi.org/10.1371/journal.pone.0142595>.
- Dietrich, J.C., Tanaka, S., Westerink, J.J., Dawson, C.N., Luettich, R.A., Zijlema, M., Holthuijsen, L.H., Smith, J.M., Westerink, L.G., Westerink, H.J., 2012. Performance of the unstructured-mesh, SWAN+ ADCIRC model in computing hurricane waves and surge. *J. Sci. Comput.* 52 (2), 468–497. <https://doi.org/10.1007/s10915-011-9555-6>.
- Dugan, J.E., Airolidi, L., Chapman, M.G., Walker, S.J., Schlacher, T., 2012. Estuarine and coastal structures: environmental effects, a focus on shore and nearshore structures. In: *Treatise On Estuarine and Coastal Science*, 8. Elsevier Inc, pp. 17–41. <https://doi.org/10.1016/B978-0-12-374711-2.00802-0>.
- Dugan, J.E., Emery, K.A., Alber, M., Alexander, C.R., Byers, J.E., Gehman, A.M., McLenaghan, N., Sojka, S.E., 2018. Generalizing ecological effects of shoreline armoring across soft sediment environments. *Estuaries Coast.* 41, 180–196. <https://doi.org/10.1007/s12237-017-0254-x>.
- Eckman, J.E., 1983. Hydrodynamic processes affecting benthic recruitment. *Limnol. Oceanogr.* 28 (2), 241–257. <https://doi.org/10.4319/lo.1983.28.2.0241>.
- Feagin, R.A., Figlus, J., Zinnert, J.C., Sigren, J., Martinez, M.L., Silva, R., Smith, W.K., Cox, D., Young, D.R., Carter, G., 2015. Going with the flow or against the grain? The promise of vegetation for protecting beaches, dunes, and barrier islands from erosion. *Front. Ecol. Environ.* 13 (4), 203–210. <https://doi.org/10.1890/140218>.
- Folke, C., 2006. Resilience: the emergence of a perspective for social-ecological systems analyses. *Glob. Environ. Change* 16 (3), 253–267. <https://doi.org/10.1016/j.gloenvcha.2006.04.002>.
- Ford, S.E., Scarpa, E., Bushek, D., 2012. Spatial and temporal variability of disease resistance in an estuary: implications for the development of resistance. *J. Mar. Res.* 70 (2–3), 253–277. <https://doi.org/10.1357/002224012802851850>.
- Fuchs, H.L., Gerbi, G.P., Hunter, E.J., Christman, A.J., Diez, F.J., 2015. Hydrodynamic sensing and behavior by oyster larvae in turbulence and waves. *J. Exp. Biol.* 218 (9), 1419–1432. <https://doi.org/10.1242/jeb.118562>.
- Fuchs, H.L., Reidenbach, M.A., 2013. Biophysical constraints on optimal patch lengths for settlement of a reef-building bivalve. *PLoS ONE* 8 (8). <https://doi.org/10.1371/journal.pone.0071506>.
- Fugate, D.C., Friedrichs, C.T., 2002. Determining concentration and fall velocity of estuarine particle populations using ADV, OBS and LISST. *Cont. Shelf Res.* 22 (11–13), 1867–1886. [https://doi.org/10.1016/S0278-4343\(02\)00043-2](https://doi.org/10.1016/S0278-4343(02)00043-2).
- Fulford, R.S., Breitburg, D.L., Newell, R.I.E., Kemp, W.M., Luckenbach, M., 2007. Effects of oyster population restoration strategies on phytoplankton biomass in Chesapeake Bay: a flexible modeling approach. *Mar. Ecol. Prog. Ser.* 336, 43–61. <https://doi.org/10.3354/meps336043>.
- Giardino, D., Bacopoulos, P., Hagen, S.C., 2011. Tidal spectroscopy of the lower St. Johns River from a high-resolution shallow water hydrodynamic model. *Int. J. Ocean Clim. Syst.* 2 (1), 1–18. <https://doi.org/10.1260/1759-3131.2.1.1>.
- Grabowski, J.H., 2004. Habitat complexity disrupts predator-prey interactions but not the trophic cascade on oyster reefs. *Ecology* 85 (4), 995–1004. <https://doi.org/10.1890/03-0067>.
- Grabowski, J.H., Brumbaugh, R.D., Conrad, R.F., Keeler, A.G., Opaluch, J.J., Peterson, C. H., Piehler, M.F., Powers, S.P., Smyth, A.R., 2012. Economic valuation of ecosystem services provided by oyster reefs. *Bioscience* 62 (10), 900–909. <https://doi.org/10.1525/bio.2012.62.10.10>.
- Grabowski, J.H., Hughes, A.R., Kimbro, D.L., Dolan, M.A., 2005. How habitat setting influences restored oyster reef communities. *Ecology* 86 (7), 1926–1935. <https://doi.org/10.1890/04-0690>.
- Grizzle, R.E., Langan, R., Hunting Howell, W., 1992. Growth responses of suspension-feeding bivalve molluscs to changes in water flow: differences between siphonate

- and nonsiphonate taxa. *J. Exp. Mar. Biol. Ecol.* 162 (2), 213–228. [https://doi.org/10.1016/0022-0981\(92\)90202-L](https://doi.org/10.1016/0022-0981(92)90202-L).
- Hagen, S.C., Zundel, A.K., Kojima, S., 2006. Automatic, unstructured mesh generation for tidal calculations in a large domain. *Int. J. Comput. Fluid Dyn.* 20 (8), 593–608. <https://doi.org/10.1080/10618560601046846>.
- Harsh, M.W., Mann, D.A., Orth, R.L., & Moore, R.J., 1995. Filtration by oysters : interactive effects of water flow, seston composition and filtration rate. <https://doi.org/10.25773/q841-vg28>.
- Hofmann, E., Ford, S., Powell, E., Klinck, J., 2001. Modeling studies of the effect of climate variability on MSX disease in eastern oyster (*Crassostrea virginica*) populations. *Hydrobiologia* 460, 195–212. <https://doi.org/10.1023/A:1013159329598>.
- Housego, R.M., Rosman, J.H., 2016. A model for understanding the effects of sediment dynamics on oyster reef development. *Estuaries Coast.* 39 (2), 495–509. <https://doi.org/10.1007/s12237-015-9998-3>.
- Jordan-Cooley, W.C., Lipcius, R.N., Shaw, L.B., Shen, J., Shi, J., 2011. Bistability in a differential equation model of oyster reef height and sediment accumulation. *J. Theor. Biol.* 289 (1), 1–11. <https://doi.org/10.1016/j.jtbi.2011.08.013>.
- Kamphuis, J.W., 2020. Introduction to coastal engineering and management, 2nd edition. Introduction to Coastal Engineering and Management, 2nd Edition, 3rd ed. World Scientific Publishing Company. <https://doi.org/10.1142/7021>.
- Kellogg, M.L., Cornwell, J.C., Owens, M.S., Paynter, K.T., 2013. Denitrification and nutrient assimilation on a restored oyster reef. *Mar. Ecol. Prog. Ser.* 480, 1–19. <https://doi.org/10.3354/meps10331>.
- Kennedy, V., Newell, R., Eble, A., 1996. *The Eastern Oyster: Crassostrea virginica*. Maryland Sea Grant College. University of Maryland System.
- Kingsley-Smith, P.R., Luckenbach, M.W., 2008. Post-settlement survival and growth of the suminoe oyster, *crassostrea ariakensis*, exposed to simulated emersion regimes. *J. Shellfish Res.* 27 (3), 609–618. [https://doi.org/10.2983/0730-8000\(2008\)27\[609:PSAGOT\]2.0.CO;2](https://doi.org/10.2983/0730-8000(2008)27[609:PSAGOT]2.0.CO;2).
- La Peyre, M.K., Serra, K., Joyner, T.A., Humphries, A., 2015. Assessing shoreline exposure and oyster habitat suitability maximizes potential success for sustainable shoreline protection using restored oyster reefs. *PeerJ* 2015 (10), e1317. <https://doi.org/10.7717/peerj.1317>.
- Lenihan, H.S., 1999. Physical-biological coupling on oyster reefs: how habitat structure influences individual performance. *Ecol. Monogr.* 69 (3), 251–275. [https://doi.org/10.1890/0012-9615\(1999\)069\[0251:PBCCOOR\]2.0.CO;2](https://doi.org/10.1890/0012-9615(1999)069[0251:PBCCOOR]2.0.CO;2).
- Lenihan, H.S., Peterson, C.H., Allen, J.M., 1996. Does flow speed also have a direct effect on growth of active suspension-feeders: an experimental test on oysters. *Limnol. Oceanogr.* 41 (6), 1359–1366. <https://doi.org/10.4319/lo.1996.41.6.1359>.
- Lenihan, H.S., Peterson, C.H., Byers, J.E., Grabowski, J.H., Thayer, G.W., Colby, D.R., 2001. Cascading of habitat degradation: oyster reefs invaded by refugee fishes escaping stress. *Ecol. Appl.* 11 (3), 764–782. [https://doi.org/10.1890/1051-0761\(2001\)011\[0764:COHDOR\]2.0.CO;2](https://doi.org/10.1890/1051-0761(2001)011[0764:COHDOR]2.0.CO;2).
- Luettich, R.A., Westerink, J.J., & Scheffner, N.W., 1992. ADCIRC: an advanced three-dimensional circulation model for shelves, coasts, and estuaries. <http://hdl.handle.net/11681/4618>.
- Luettich, R., & Westerink, J.J., 2004. Formulation and numerical implementation of the 2D/3D ADCIRC finite element model version 44. XX. 1–74.
- McCowan, J., 1894. On the highest wave of permanent type. *Lond. Edinb. Dublin Philos. Mag. J. Sci.* 38 (233), 351–358. <https://doi.org/10.1080/1478644908620643>.
- Meyer, D.L., Townsend, E.C., Thayer, G.W., 1997. Stabilization and erosion control value of oyster cultch for intertidal marsh. *Restor. Ecol.* 5 (1), 93–99. <https://doi.org/10.1046/j.1526-100X.1997.09710.x>.
- Michener, W.K., Kenny, P.D., 1991. Spatial and temporal patterns of *Crassostrea virginica* (Gmelin) recruitment: relationship to scale and substratum. *J. Exp. Mar. Biol. Ecol.* 154 (1), 97–121. [https://doi.org/10.1016/0022-0981\(91\)90077-A](https://doi.org/10.1016/0022-0981(91)90077-A).
- Morris, R.L., Bilkovic, D.M., Boswell, M.K., Bushek, D., Cebrian, J., Goff, J., Kibler, K.M., La Peyre, M.K., McClenachan, G., Moody, J., Sacks, P., Shinn, J.P., Sparks, E.L., Temple, N.A., Walters, L.J., Webb, B.M., Swearer, S.E., 2019. The application of oyster reefs in shoreline protection: are we over-engineering for an ecosystem engineer? *J. Appl. Ecol.* 56 (7), 1703–1711. <https://doi.org/10.1111/1365-2664.13390>.
- Morris, R.L., Konlechner, T.M., Ghisalberti, M., Swearer, S.E., 2018. From grey to green: efficacy of eco-engineering solutions for nature-based coastal defence. *Glob. Chang. Biol.* 24 (5), 1827–1842. <https://doi.org/10.1111/gcb.14063>.
- Morris, R.L., La Peyre, M.K., Webb, B.M., Marshall, D.A., Bilkovic, D.M., Cebrian, J., McClenachan, G., Kibler, K.M., Walters, L.J., Bushek, D., Sparks, E.L., Temple, N.A., Moody, J., Angstadt, K., Goff, J., Boswell, M., Sacks, P., Swearer, S.E., 2021. Large-scale variation in wave attenuation of oyster reef living shorelines and the influence of inundation duration. *Ecol. Appl.* 31 (6) <https://doi.org/10.1002/eap.2382>.
- Motes, M.L., DePaola, A., Cook, D.W., Veazey, J.E., Hunsucker, J.C., Garthright, W.E., Blodgett, R.J., Chirtel, S.J., 1998. Influence of water temperature and salinity on *Vibrio vulnificus* in Northern Gulf and Atlantic Coast oysters (*Crassostrea virginica*). *Appl. Environ. Microbiol.* 64 (4), 1459–1465. <https://doi.org/10.1128/aem.64.4.1459-1465.1998>.
- Munroe, D.M., Powell, E.N., Ford, S.E., Hofmann, E.E., Klinck, J.M., 2015. Outcomes of asymmetric selection pressure and larval dispersal on evolution of disease resistance: a metapopulation modeling study with oysters. *Mar. Ecol. Prog. Ser.* 531, 221–239. <https://doi.org/10.3354/meps11349>.
- Nadal-Caraballo, N.C., Campbell, M.O., Gonzalez, V.M., Torres, M.J., Melby, J.A., Tafiandis, A.A., 2020. Coastal hazards system: a probabilistic coastal hazard analysis framework. *J. Coast. Res.* 95 (sp1), 1211–1216. <https://doi.org/10.2112/S195-235.1>.
- Newell, R.I.E., Fisher, T.R., Holyoke, R.R., Cornwell, J.C., 2005. Influence of eastern oysters on nitrogen and phosphorus regeneration in Chesapeake Bay, USA. The Comparative Roles of Suspension-Feeders in Ecosystems. Springer-Verlag, pp. 93–120. https://doi.org/10.1007/1-4020-3030-4_6.
- Newell, R.I.E., Koch, E.W., 2004. Modeling seagrass density and distribution in response to changes in turbidity stemming from bivalve filtration and seagrass sediment stabilization. *Estuaries* 27 (5), 793–806. <https://doi.org/10.1007/BF02912041>.
- Nordstrom, K.F., 2014. Living with shore protection structures: a review. *Estuar. Coast. Shelf Sci.* 150 (PA), 11–23. <https://doi.org/10.1016/j.eccs.2013.11.003>.
- Peralta, G., Pérez-Lloréns, J.L., Hernández, I., Brun, F., Vergara, J.J., Bartual, A., Gálvez, J.A., García, C.M., 2000. Morphological and physiological differences between two morphotypes of *Zostera noltii* Hornem. From the south-western Iberian Peninsula. *Helgol. Mar. Res.* 54 (2–3), 80–86. <https://doi.org/10.1007/s101520050005>.
- Powell, E.N., Klinck, J.M., Guo, X., Hofmann, E.E., Ford, S.E., Bushek, D., 2012. Can oysters *crassostrea virginica* develop resistance to dermo disease in the field: the impediment posed by climate cycles. *J. Mar. Res.* 70 (2–3), 309–355. <https://doi.org/10.1357/002224012802851896>.
- Powers, S.P., Peterson, C.H., Grabowski, J.H., Lenihan, H.S., 2009. Success of constructed oyster reefs in no-harvest sanctuaries: implications for restoration. *Mar. Ecol. Prog. Ser.* 389, 159–170.
- Rose, C.D., 1973. Mortality of market-sized oysters (*Crassostrea virginica*) in the vicinity of a dredging operation. *Chesapeake Sci.* 14 (2), 135–138. <https://doi.org/10.2307/1350880>.
- Schoonees, T., Gijón Mancheño, A., Scheres, B., Bouma, T.J., Silva, R., Schlurmann, T., Schüttrumpf, H., 2019. Hard structures for coastal protection, towards greener designs. *Estuaries Coast.* 42 (7), 1709–1729. <https://doi.org/10.1007/s12237-019-00551-z>.
- Schulte, D.M., Burke, R.P., Lipcius, R.N., 2009. Unprecedented restoration of a native oyster metapopulation. *Science* 325 (5944), 1124–1128. <https://doi.org/10.1126/science.1176516>.
- Scyphers, S.B., Powers, S.P., Heck, K.L., Byron, D., 2011a. Oyster reefs as natural breakwaters mitigate shoreline loss and facilitate fisheries. *PLoS ONE* 6 (8), e22396. <https://doi.org/10.1371/journal.pone.0022396>.
- Scyphers, S.B., Powers, S.P., Heck, K.L., Byron, D., Jr, K.L.H., Byron, D., Heck, K.L., Byron, D., 2011b. Oyster reefs as natural breakwaters mitigate shoreline loss and facilitate fisheries. *PLoS ONE* 6 (8), e22396. <https://doi.org/10.1371/journal.pone.0022396>.
- Shepard, C.C., Crain, C.M., Beck, M.W., 2011. The protective role of coastal marshes: a systematic review and meta-analysis. *PLoS ONE* 6 (11), e23734. <https://doi.org/10.1371/journal.pone.0027374>. Public Library of Science.
- Shields, A., 1936. Anwendung der Aehnlichkeitsmechanik und der Turbulenzforschung auf die Geschiebebewegung. *Technology (Singap. World Sci.)* 26 (1).
- Skilleter, G.A., Peterson, C.H., 1994. Control of foraging behavior of individuals within an ecosystem context: the clam *Macoma balthica* and interactions between competition and siphon cropping. *Oecologia* 100 (3), 268–278. <https://doi.org/10.1007/BF00316954>.
- Smyth, A.R., Gerald, N.R., Piehler, M.F., 2013. Oyster-mediated benthic-pelagic coupling modifies nitrogen pools and processes. *Mar. Ecol. Prog. Ser.* 493, 23–30. <https://doi.org/10.3354/meps10516>.
- Temmerman, S., Meire, P., Bouma, T.J., Herman, P.M.J., Ysebaert, T., De Vriend, H.J., 2013. Ecosystem-based coastal defence in the face of global change. *Nature* 504 (7478), 79–83. <https://doi.org/10.1038/nature12859>.
- U.S. Geological Survey. (2020). *usSEABED* (usSEABED: offshore surficial-sediment database for samples collected within the United States exclusive economic zone). <https://cmgds.marine.usgs.gov/usseabed/#home>.
- van Rijn, L.C., 1993. Principles of sediment transport in rivers, estuaries and coastal seas. *Principles of Sediment Transport in Rivers, Estuaries and Coastal Seas*, pp. 1–17.
- Walker, B., Holling, C.S., Carpenter, S.R., Kinzig, A., 2004. Resilience, adaptability and transformability in social-ecological systems. *Ecol. Soc.* 9 (2) <https://doi.org/10.5751/ES-00650-090205>.
- Webb, P., 2017. Wave basics. Introduction to Oceanography. <https://rwu.pressbooks.pub/webboceanography/>.
- Wellman, E.H., Baillie, C.J., Puckett, B.J., Donaher, S.E., Trackenberg, S.N., Gittman, R. K., 2022. Reef design and site hydrodynamics mediate oyster restoration and marsh stabilization outcomes. *Ecol. Appl.* 32 (2) <https://doi.org/10.1002/eap.2506>.
- Wentworth, C.K., 1922. A scale of grade and class terms for clastic sediments. *J. Geol.* 30 (5), 377–392. <https://doi.org/10.1086/622910>.
- Whitman, E.R., Reidenbach, M.A., 2012. Benthic flow environments affect recruitment of *Crassostrea virginica* larvae to an intertidal oyster reef. *Mar. Ecol. Prog. Ser.* 463, 177–191. <https://doi.org/10.3354/meps09882>.
- Wiberg, P.L., Taube, S.R., Ferguson, A.E., Kremer, M.R., Reidenbach, M.A., 2018. Wave attenuation by oyster reefs in shallow coastal bays. *Estuaries Coast.* 42 (2), 331–347. <https://doi.org/10.1007/s12237-018-0463-y>.
- Zu Ermgassen, P.S.E., Spalding, M.D., Blake, B., Coen, L.D., Dumbauld, B., Geiger, S., Grabowski, J.H., Grizzle, R., Luckenbach, M., McGraw, K., Rodney, W., Ruesink, J.L., Powers, S.P., Brumbaugh, R., 2012. Historical ecology with real numbers: past and present extent and biomass of an imperilled estuarine habitat. *Proc. R. Soc. B: Biol. Sci.* 279 (1742), 3393–3400. <https://doi.org/10.1098/rspb.2012.0313>.